Article

Cell Reports

Metabolic Interplay between Astrocytes and Neurons Regulates Endocannabinoid Action

Graphical Abstract

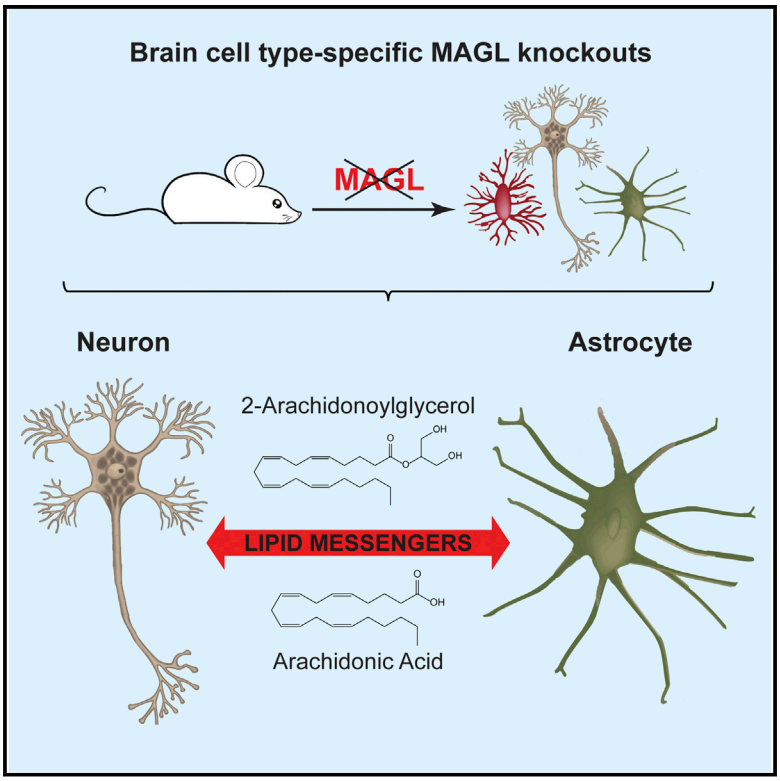

Authors

Andreu Viader, Jacqueline L. Blankman, Peng Zhong, ..., Dana E. Selley, Laura J. Sim-Selley, Benjamin F. Cravatt

Correspondence

cravatt@scripps.edu

In Brief

The endocannabinoid 2-arachidonoylglycerol (2-AG) is a retrograde lipid messenger that broadly modulates brain synapses, neurophysiology, and behavior. Viader et al. show that endocannabinoid signaling is regulated by the cooperative, transcellular metabolism of 2-AG, which is shuttled between neurons and astrocytes.

Highlights

- Genetic mouse models reveal cellular specificity of 2-AG metabolism
- Astrocytes and neurons collaborate to terminate endocannabinoid signaling
- Coordinated astrocytic-neuronal metabolism protects against CB_1R desensitization
- Astrocytes couple 2-AG hydrolysis to neuroinflammatory prostaglandin production

Viader et al., 2015, Cell Reports *12*, 798–808
August 4, 2015
http://dx.doi.org/10.1016/j.celrep.2015.06.075

OPEN ACCESS
CellPress

Cell Reports
Article

Metabolic Interplay between Astrocytes and Neurons Regulates Endocannabinoid Action

Andreu Viader,[1,2] Jacqueline L. Blankman,[3] Peng Zhong,[4] Xiaojie Liu,[4] Joel E. Schlosburg,[5] Christopher M. Joslyn,[1,2] Qing-Song Liu,[4] Aaron J. Tomarchio,[6] Aron H. Lichtman,[6] Dana E. Selley,[6] Laura J. Sim-Selley,[6] and Benjamin F. Cravatt[1,2,*]

[1]The Skaggs Institute for Chemical Biology
[2]Department of Chemical Physiology
The Scripps Research Institute, La Jolla, CA 92037, USA
[3]Abide Therapeutics, San Diego, CA 92121, USA
[4]Department of Pharmacology and Toxicology, Medical College of Wisconsin, Milwaukee, WI 53226, USA
[5]Committee on the Neurobiology of Addictive Disorders, The Scripps Research Institute, La Jolla, CA 92037, USA
[6]Department of Pharmacology and Toxicology, Virginia Commonwealth University, Richmond, VA 23298, USA
*Correspondence: cravatt@scripps.edu
http://dx.doi.org/10.1016/j.celrep.2015.06.075

SUMMARY

The endocannabinoid 2-arachidonoylglycerol (2-AG) is a retrograde lipid messenger that modulates synaptic function, neurophysiology, and behavior. 2-AG signaling is terminated by enzymatic hydrolysis—a reaction that is principally performed by monoacylglycerol lipase (MAGL). MAGL is broadly expressed throughout the nervous system, and the contributions of different brain cell types to the regulation of 2-AG activity in vivo remain poorly understood. Here, we genetically dissect the cellular anatomy of MAGL-mediated 2-AG metabolism in the brain and show that neurons and astrocytes coordinately regulate 2-AG content and endocannabinoid-dependent forms of synaptic plasticity and behavior. We also find that astrocytic MAGL is mainly responsible for converting 2-AG to neuroinflammatory prostaglandins via a mechanism that may involve transcellular shuttling of lipid substrates. Astrocytic-neuronal interplay thus provides distributed oversight of 2-AG metabolism and function and, through doing so, protects the nervous system from excessive CB_1 receptor activation and promotes endocannabinoid crosstalk with other lipid transmitter systems.

INTRODUCTION

Historical neuron-centric conceptualizations of brain function have given way to a deeper appreciation of the important roles played by additional brain cell types in regulating chemical transmission throughout the nervous system (McIver et al., 2013). Astrocytes are now recognized as integral components of synapses and central regulators of neurotransmission and interneuronal communication (Halassa and Haydon, 2010). Astroglial transporters clear neurotransmitters, such as glutamate and γ-amino butyric acid (GABA), from synaptic clefts to modulate the signaling activities of these chemical messengers and limit their toxic accumulation in the extracellular space (Danbolt, 2001). Metabolic pathways in astrocytes are also essential for the recycling and resupply of neurotransmitters needed to maintain sustained rounds of synaptic activity (Coulter and Eid, 2012). Moreover, defects in astrocytic functions that lead to alterations in the homeostasis of major neurotransmitters have been linked to a variety of mental and neurodegenerative disorders (Allaman et al., 2011; Halassa and Haydon, 2010). Microglia, which are resident immune cells of the nervous system, also contribute to neurotransmission through activity-dependent remodeling and pruning of synapses (Salter and Beggs, 2014; Schafer et al., 2012). Efforts to elucidate the contributions of glia to the regulation of synaptic function therefore stand to both enrich our mechanistic understanding of intercellular communication in the brain and provide new therapeutic avenues for the treatment of diverse neurological conditions.

The endogenous cannabinoid (endocannabinoid or eCB) 2-arachidonoylglycerol (2-AG) is an arachidonic acid (AA)-derived retrograde lipid messenger that broadly modulates synaptic function throughout the nervous system (Fowler et al., 2005; Kano et al., 2009; Pacher et al., 2006). 2-AG is synthesized by diacylglycerol lipases (DAGLs) (Reisenberg et al., 2012) and released in an activity-dependent manner from postsynaptic neurons to act on presynaptic G-protein-coupled cannabinoid receptors CB_1 (CB_1R) and CB_2, which are also targets of the primary psychoactive component of marijuana (Δ^9-tetrahydrocannabinol) (Mechoulam and Hanus, 2000). Principally through its activity on CB_1Rs, 2-AG inhibits neurotransmitter release and regulates diverse neurophysiological processes, including mood, nociception, appetite, and memory (Pacher et al., 2006). Enzymatic hydrolysis of 2-AG, which is primarily mediated by monoacylglycerol lipase (MAGL) in the nervous system (Dinh et al., 2002; Ueda et al., 2013), terminates CB_1R-dependent signaling (Chanda et al., 2010; Schlosburg et al., 2010; Zhong et al., 2011) and concomitantly provides a major source of AA

for brain eicosanoid synthesis (Nomura et al., 2011). The DAGL and MAGL enzymes thus tightly regulate 2-AG-mediated neurotransmission and have historically been viewed as doing so through their respective expression in the pre- and post-synaptic compartments of neurons (Di Marzo et al., 2015). Glial cells may also serve as cellular substrates for the modulation of 2-AG, however, as both astrocytes and microglia release this eCB and express CB_1Rs (Navarrete and Araque, 2008, 2010; Stella, 2010; Walter et al., 2004; Witting et al., 2004). Furthermore, ectopic expression of MAGL in Bergmann glia has been shown to attenuate 2-AG-dependent retrograde synaptic suppression in cerebellar slices from MAGL$^{-/-}$ mice (Tanimura et al., 2012). Nonetheless, the relative contributions of neurons and glia to the termination of 2-AG-dependent synaptic and neurobehavioral functions, as well as the potential for crosstalk between these cell types to facilitate the recycling and homeostasis of eCB-eicosanoid pools, remain largely unexplored.

Global pharmacological or genetic disruption of MAGL robustly elevates brain 2-AG content (Chanda et al., 2010; Long et al., 2009; Schlosburg et al., 2010), alters CB_1R-mediated signaling and behaviors (Chanda et al., 2010; Long et al., 2009; Schlosburg et al., 2010; Zhong et al., 2011), and impairs neuroinflammation through mechanisms that involve eCB-eicosanoid crosstalk (Nomura et al., 2011). With the goal of determining the relative contribution of different brain cell types to 2-AG metabolism and signaling in vivo, we report the generation and characterization of a conditional genetic mouse model used to ablate MAGL globally and specifically in neurons, astrocytes, and microglia. We discover that neuronal and astrocytic MAGL coordinately regulate brain 2-AG content, contribute to the termination of synaptic 2-AG signaling at CB_1Rs, and, by doing so, maintain a balanced eCB tone that protects against desensitization caused by excessive signaling. Moreover, we show that astrocytic MAGL is principally responsible for generating 2-AG-derived arachidonate pools used for the synthesis of pro-inflammatory prostaglandins in the brain. Finally, we provide evidence for the transcellular shuttling of 2-AG and related metabolites between neurons and astrocytes as one mechanism by which these cells can coordinately regulate eCB-eicosanoid pathways in the nervous system. The distributed metabolism of 2-AG across both neurons and astrocytes thus affords the nervous system more refined control over dynamic features of eCB activity, including protection against desensitization and facilitating crosstalk with other lipid transmitter systems that are deregulated in disease states.

RESULTS

Cell-Type-Specific Deletion of MAGL in the Nervous System

To examine the contribution of different brain cell types to 2-AG metabolism and signaling in vivo, we generated a genetic mouse model for conditional deletion of the MAGL enzyme by flanking the catalytic exon of the *Mgll* gene (exon 4, containing catalytic S122) with *loxP* recombination sites (MAGL^{loxP}, Figures 1A and S1A–S1C). The MAGL^{loxP} line was initially validated by crossing to mice that ubiquitously express Cre recombinase (Rosa26-Cre; Otto et al., 2009) to produce total MAGL$^{-/-}$ mice (MAGL-TKO). Consistent with previous reports for other conventional MAGL$^{-/-}$ lines (Chanda et al., 2010; Schlosburg et al., 2010), MAGL-TKO mice lacked detectable MAGL expression and activity across different central and peripheral tissues and cell types (Figures 1B–1E and S1D). MAGL-TKO mice also exhibited marked (~90%) reductions in brain 2-AG hydrolysis (Figure 1F), as well as ~10-fold elevations in brain 2-AG content (Figure 1G).

We next crossed homozygous MAGL^{loxP} mice to mice with restricted expression of Cre recombinase in neurons (Eno2-Cre; Frugier et al., 2000), astrocytes (GFAP-Cre; Tao et al., 2011), or microglia (LysM-Cre; Clausen et al., 1999) to generate mouse lines that lack MAGL specifically in these three brain cell types (MAGL-NKO, MAGL-AKO, and MAGL-MKO, respectively). Crossing of Eno2-, GFAP-, and LysM-cre mice to a Cre-inducible Rosa26-tdTomato reporter line validated efficient Cre-mediated recombination throughout the brain of these animals, selectively in neurons, astrocytes, and microglia, respectively (Figure S1E). While the Eno2- and GFAP-Cre lines produced Cre-mediated recombination in the vast majority (80–90+%) of neurons and astrocytes, respectively (with the GFAP-Cre line also showing low-level (~2%–6%) recombination in neurons, consistent with previous studies; Tao et al., 2011), the LysM-Cre line only appeared to promote Cre-mediated recombination in ~50%–60% of Iba1-positive microglia in the brain. Cultured preparations of brain cells (Figure S1F and S1G), however, confirmed selective and near-complete loss of MAGL expression in microglia from MAGL-MKO mice, as well as in neurons (GABAergic and glutamatergic; Figure S1H) and astrocytes from MAGL-NKO and MAGL-AKO, respectively (Figure 1B). Importantly, each MAGL-disrupted brain cell type also displayed significantly reduced 2-AG hydrolytic activity, although the relative magnitude of this decrease was greater for neurons compared to astrocytes or microglia, possibly due to the presence of additional 2-AG hydrolases in glia (Marrs et al., 2010; Figure 1C).

Having established mouse models that display selective loss of MAGL in different brain cell types, we next examined how neurons, astrocytes, and microglia contribute to bulk 2-AG metabolism in the nervous system. Deletion of MAGL in both neurons and astrocytes, but not microglia, substantially reduced the total quantity of active enzyme in brain tissue, as measured by activity-based protein profiling (ABPP; Figures 1D and 1E). These data mirrored the effects on brain 2-AG hydrolysis, which was decreased by ~60% and 40% in MAGL-NKO and MAGL-AKO mice, respectively, but unaltered in MAGL-MKO mice (Figure 1F). Notably, both MAGL-NKO and MAGL-AKO mice displayed significant (~5- and 3-fold, respectively) increases in brain 2-AG (Figure 1G). No changes in brain 2-AG content were found in MAGL-MKO mice. Finally, none of the conditional MAGL$^{-/-}$ mouse lines displayed alterations in anandamide (AEA) (Figure 1H), a second major eCB that is principally hydrolyzed by fatty acid amide hydrolase (Cravatt et al., 1996). These data, taken together, indicate that both neuronal and astrocytic MAGL make substantial contributions to 2-AG metabolism in the brain.

Neuronal and Astrocytic MAGL Regulate eCB-Dependent Synaptic Plasticity

2-AG functions as a major retrograde synaptic messenger that suppresses neurotransmitter release after binding to presynaptic

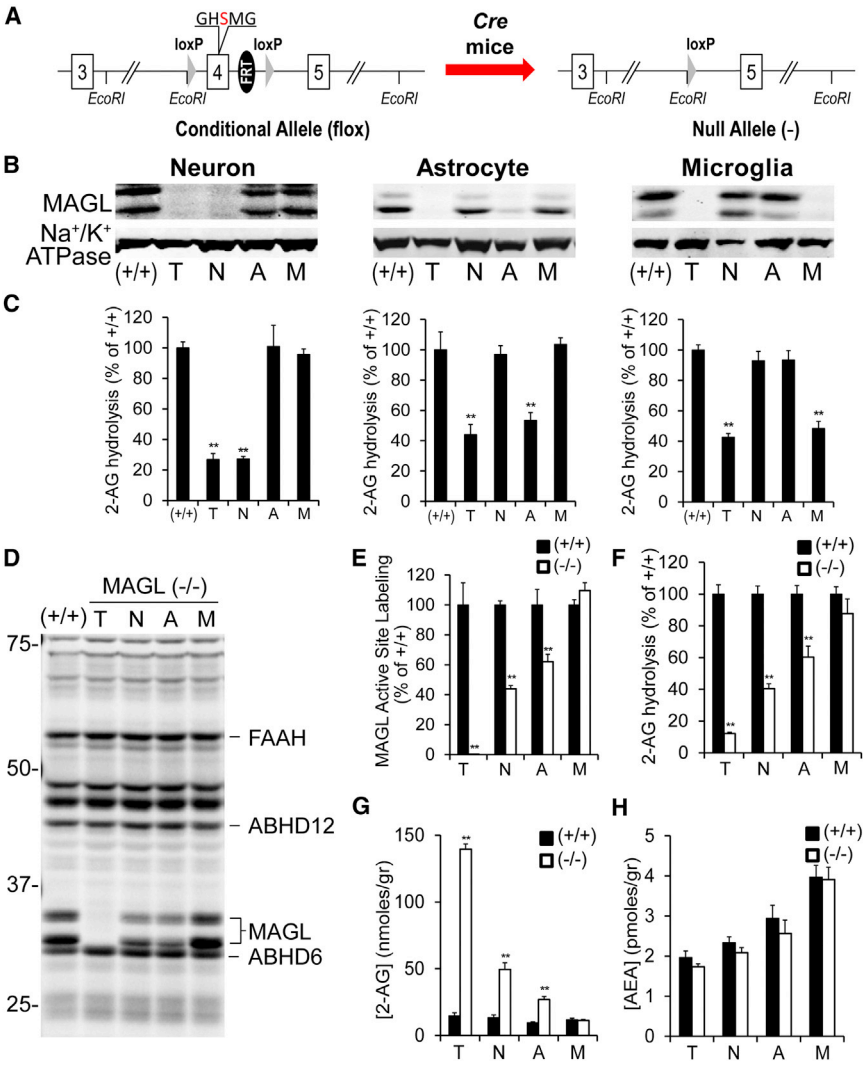

Figure 1. Brain Cell Type-Specific Deletion of MAGL Identifies Both Neurons and Astrocytes as Key Regulators of 2-AG Metabolism in the Nervous System

(A) Diagram of the targeted *Mgll* locus in MAGL^{loxP} mice, in which the catalytic exon 4 of this enzyme is flanked by *loxP* recombination sites (GHSMG sequence containing the catalytic serine nucleophile is shown). When MAGL^{loxP} mice are crossed with mice that express Cre recombinase, exon 4 is excised to produce the null allele (MAGL^{-}).

(B) Western blot of neurons, astrocytes, and microglia derived from MAGL-TKO (T, total), MAGL-NKO (N, neuron), MAGL-AKO (A, astrocyte), or MAGL-MKO (M, microglia) mice confirms efficient and cell-type-specific depletion of MAGL in these different mouse lines.

(C) 2-AG hydrolytic activities of neuron, astrocyte, and microglia membrane proteomes derived from MAGL-TKO (T), MAGL-NKO (N), MAGL-AKO (A), and MAGL-MKO (M) mice confirms cell-type-specific loss of MAGL in these different mice. n = 4–5 per cell type and genotype. Error bars represent SEM; $^{**}p < 0.01$ versus MAGL$^{+/+}$ samples.

(D and E) SDS-PAGE readout of an activity-based protein profiling (ABPP) analysis of brain membrane proteomes from MAGL-TKO (T), MAGL-NKO (N), MAGL-AKO (A), and MAGL-MKO (M) mice using a serine-hydrolase-directed fluorophosphonate-rhodamine probe (Cravatt et al., 2008) (fluorescent gel shown in grayscale) (D). Quantification of MAGL band intensity is shown (E). n = 4–5 mice per genotype. Error bars represent SEM; $^{**}p < 0.01$ versus MAGL$^{+/+}$ samples.

(F) 2-AG hydrolytic activities of MAGL-TKO (T), MAGL-NKO (N), MAGL-AKO (A), and MAGL-MKO (M) brain membrane proteomes. n = 4–5 mice per genotype. Error bars represent SEM; $^{**}p < 0.01$ versus MAGL$^{+/+}$ samples.

(G and H) Brain levels of 2-AG (G) and anandamide (AEA, H) in MAGL-TKO (T), MAGL-NKO (N), MAGL-AKO (A), and MAGL-MKO (M) mice. n = 8 mice per genotype. Error bars represent SEM; $^{**}p < 0.01$ versus MAGL$^{+/+}$ samples.

See also Figure S1.

CB_1Rs (Kano et al., 2009). Various forms of synaptic plasticity are regulated by retrograde eCB signaling, including depolarization-induced suppression of excitation (DSE) and inhibition (DSI) (Kano et al., 2009). Complete genetic or pharmacological ablation of MAGL activity significantly prolongs DSE/DSI (Pan et al., 2009; Straiker et al., 2009; Zhong et al., 2011), and the selective ablation of MAGL in cerebellar granule cells also extends DSE, but to a lesser degree than global ablation of the enzyme (Tanimura et al., 2012). To more clearly delineate the relative control that different brain cell types exert over 2-AG-dependent forms of synaptic plasticity, we initially examined DSE at parallel fiber (PF) to Purkinje cell (PC) synapses in acute cerebellar slices prepared from the different conditional MAGL-knockout lines.

A brief depolarization of PCs induced robust transient DSE at PF-PC synapses in MAGL$^{+/+}$ cerebellar slices (Figures 2A–2C). Consistent with previous reports (Tanimura et al., 2012; Zhong et al., 2011), global deletion of MAGL substantially prolonged the duration (Figure 2A), but not magnitude (Figure S2A), of DSE at PF-PC synapses in MAGL-TKO mice. A less dramatic but significant DSE extension was also observed in cerebellar slices from MAGL-NKO mice (Figure 2B). Notably, cerebellar slices from MAGL-AKO mice also showed a significant prolongation in DSE (Figure 2C) that was nearly identical in total duration to that observed in MAGL-NKO slices, as indicated by changes in the mean decay time constant (τ) (Figure 2D). No differences in DSE were evident in MAGL-MKO mice (Figure S2B).

We further examined the contributions of neurons and astrocytes to CB_1R-mediated forms of synaptic plasticity by assessing DSI at CA1 pyramidal neuron synapses in hippocampal slices prepared from MAGL-TKO, MAGL-NKO, and MAGL-AKO, mice, as well as their wild-type littermates. DSI was readily induced in MAGL$^{+/+}$ CA1 pyramidal neurons by applying a brief depolarization while evoking inhibitory postsynaptic currents (IPSCs) through stimulation of synaptic inhibitory inputs (see Experimental Procedures; Figures 2E–2G). Consistent with previous

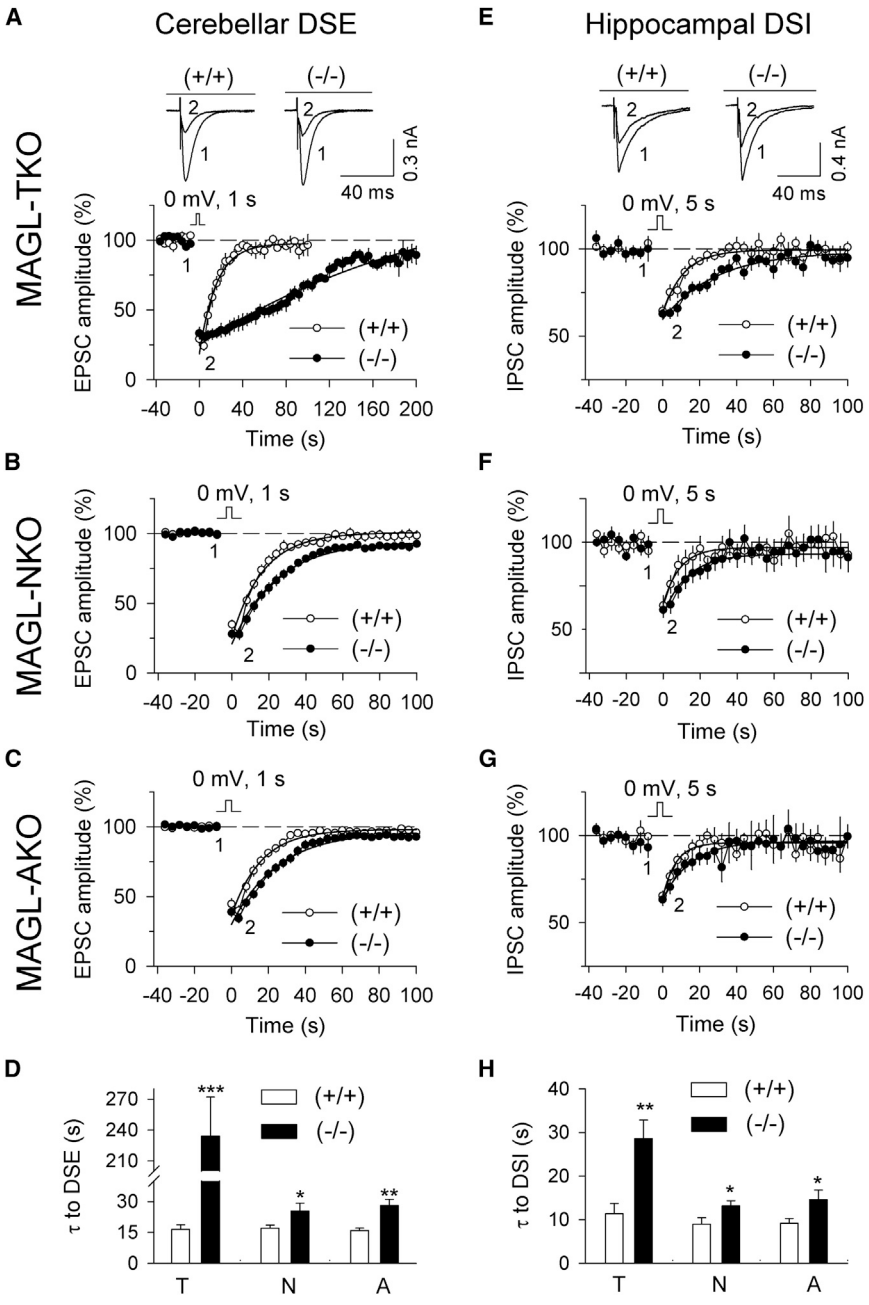

Figure 2. Astrocytic and Neuronal MAGL Play Complementary Roles in Terminating Retrograde 2-AG Signaling

(A–C) Average time courses of PF-EPSCs in response to a brief depolarization in cerebellar slices prepared from MAGL-TKO (A), MAGL-NKO (B), and MAGL-AKO (C) mice and their wild-type littermates show prolonged DSE following global, neuron- or astrocyte-specific loss of MAGL. Sample traces are shown for MAGL-TKO mice. n = 14–18 cells from n = 3 mice per genotype.

(D) Time constant (τ) of DSE in cerebellar slices prepared from MAGL-TKO (T), MAGL-NKO (N), and MAGL-AKO (A) mice and their wild-type littermates. n = 14–18 cells from n = 3 mice per genotype. Error bars represent SEM; *p < 0.05, **p < 0.01, ***p < 0.001 versus MAGL$^{+/+}$.

(E–G) Average time courses of IPSCs in CA1 pyramidal neurons in response to a brief depolarization in hippocampal slices prepared from MAGL-TKO (E), MAGL-NKO (F), and MAGL-AKO (G) mice and their wild-type littermates show prolonged DSI following global, neuron- or astrocyte-specific loss of MAGL. Sample traces are shown for MAGL-TKO mice. n = 13–15 cells from n = 3 mice per genotype.

(H) Time constant (τ) of DSI in hippocampal slices prepared from MAGL-TKO (T), MAGL-NKO (N), and MAGL-AKO (A) mice and their wild-type littermates. n = 13–15 cells from n = 3 mice per genotype. Error bars represent SEM; *p < 0.05, **p < 0.01 versus MAGL$^{+/+}$.

See also Figure S2.

reports (Pan et al., 2011), the duration of hippocampal DSI in MAGL-TKO mice was substantially prolonged (Figure 2E). Significant, albeit less dramatic, extensions in DSI were also observed in hippocampal slices from MAGL-NKO and MAGL-AKO mice (Figures 2F and 2G), both of which displayed similar increases in τ (Figure 2H).

These findings, taken together, indicate that astrocytes and neurons both play prominent roles in terminating 2-AG signaling at synaptic terminals, and, as a result, dramatic increases in the duration of CB_1R activation are only observed when MAGL is deleted from both brain cell types.

Neuronal and Astrocytic MAGL Regulate Functional CB_1R Adaptations In Vivo

Chronic, global inactivation of MAGL, achieved by either genetic disruption or repeated treatment with a MAGL inhibitor, has been shown to produce behavioral tolerance in pain models, cross-tolerance to exogenous cannabinoids, and desensitization and downregulation of brain CB_1Rs (Chanda et al., 2010; Schlosburg et al., 2010). In agreement with these earlier reports, we found that the antinociceptive and hypothermic effects of the CB_1R agonist WIN55,212-2 were substantially attenuated in MAGL-TKO mice compared to their wild-type littermates (Figures 3A and 3B). No evidence of cross-tolerance to WIN55,212-2 was observed in either MAGL-NKO or MAGL-AKO mice (Figures 3C–3F). Correlating with these behavioral data, MAGL-TKO mice, but not MAGL-NKO or MAGL-AKO mice, showed a dramatic reduction in brain CB_1R function, as measured by CB_1R agonist (CP55,940)-stimulated [^{35}S]-GTPγS binding (Figures 3G–3I). These results indicate that expression of MAGL in either neurons or astrocytes is sufficient to prevent excessive activation and corresponding desensitization of brain CB_1Rs in vivo, highlighting the contribution that

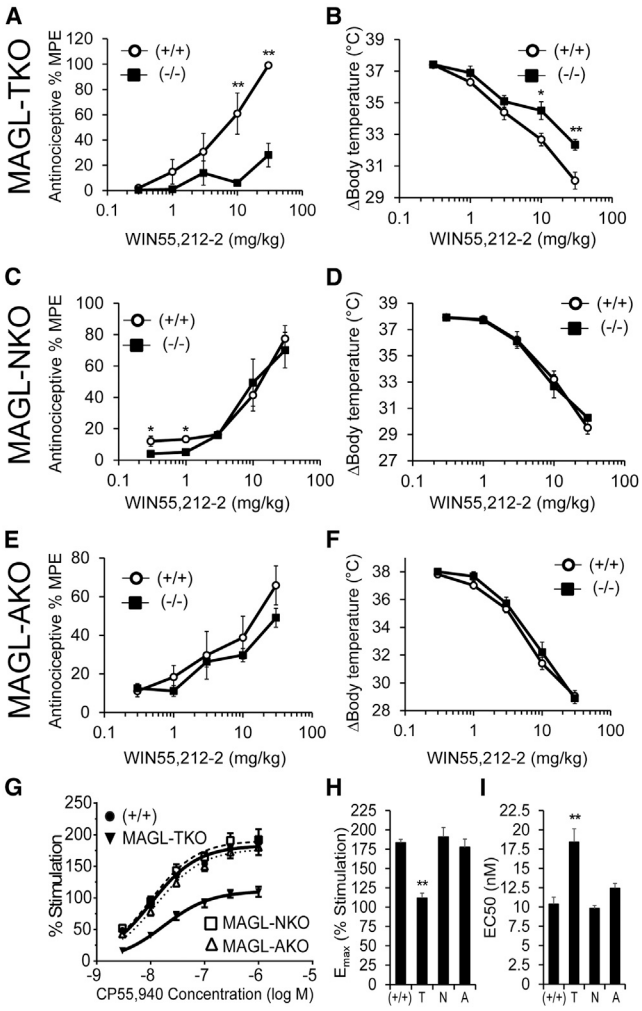

Figure 3. Astrocytic and Neuronal MAGL Maintain a Balanced eCB Tone to Protect against CB_1R Desensitization

(A–F) Antinociceptive and hypothermic effects of full CB_1R agonist WIN55,212-2 in MAGL-disrupted mice. MAGL-TKOs (A and B), but not MAGL-NKO (C and D) or MAGL-AKOs (E and F), display significant cross-tolerance to WIN55,212-2-induced antinociception and hypothermia. n = 7–8 mice per group. Error bars represent SEM; *p < 0.05 and **p < 0.01 versus wild-type littermates.

(G–I) CP55,940-stimulated [^{35}S]-GTPγS binding in hippocampal homogenates from MAGL-TKO, MAGL-NKO, and MAGL-AKO mice presented as concentration-effect curves (G) and E_{max} (H) or EC_{50} (I) values determined by nonlinear regression. n = 5 mice per group assayed in triplicate. Error bars represent SEM; **p < 0.01 versus $MAGL^{+/+}$ samples.

both cell types make to 2-AG metabolism and the maintenance of eCB signaling tone.

Astrocytes Are Critical Mediators of eCB-Eicosanoid Crosstalk

MAGL serves as a metabolic hub linking eCB and eicosanoid signaling pathways in the brain, where the hydrolysis of 2-AG provides a major source of AA substrate for prostaglandin synthesis (Nomura et al., 2011). MAGL blockade has been shown to coordinately elevate 2-AG and lower eicosanoid content in the nervous system under basal and neuroinflammatory states, including in disease models of parkinsonism and Alzheimer's disease (Chen et al., 2012; Nomura et al., 2011; Piro et al., 2012). Despite these advances in our understanding of eCB-eicosanoid crosstalk, how this interplay is enacted at the cellular level in the nervous system remains unknown. We set out to address this important question by first assessing the integrity of the eCB-prostaglandin network in individual brain cell types. Cultured neurons lacking MAGL showed significant elevations in 2-AG and reductions in AA, but, interestingly, did not produce detectable levels of prostaglandins (Figures 4A–4C). In contrast, $MAGL^{-/-}$ astrocytes, while displaying a more modest relative increase in 2-AG compared to neurons, proved capable of translating their heightened eCB content into corresponding reductions in AA and prostaglandins (Figures 4A–4C). These findings indicate that individual brain cell types, despite expressing prostaglandin biosynthetic enzymes in culture (Hewett et al., 2000; Ikeda-Matsuo et al., 2005), differ in their capacity to autonomously convert eCBs to prostaglandins, raising the possibility that this process involves transcellular metabolism in vivo.

A broader analysis of brain lipids revealed that, as expected based on previous studies (Nomura et al., 2011), global inactivation of MAGL not only elevated 2-AG but also lowered AA and prostaglandins (Figure 4D). MAGL-TKO mice also displayed markedly blunted induction of prostaglandin synthesis following lipopolysaccharide (LPS) administration compared to their $MAGL^{+/+}$ littermates (Figure 4D). In contrast, MAGL-NKO mice, despite showing ~5-fold elevations in brain 2-AG, exhibited negligible changes in AA or prostaglandin content under basal conditions or following LPS treatment (Figure 4E). MAGL-AKO mice, on the other hand, while exhibiting a more modest increase in brain 2-AG (~3-fold), showed significantly reduced brain AA content and attenuated prostaglandin production following LPS treatment (Figure 4F). Basal changes in brain prostaglandins were not observed in MAGL-AKO mice and the magnitude of decrease in these eicosanoids following LPS treatment was less substantial than that observed in MAGL-TKO mice (Figures 4D and 4F).

LPS treatment, in addition to inducing brain prostaglandin synthesis, stimulates an acute neuroinflammatory response as reflected in microglial activation and cytokine production. Consistent with previous findings, MAGL-TKO mice showed significant reductions in LPS-induced brain cytokines and microglial activation compared to $MAGL^{+/+}$ littermates (Figure S3A–S3D). These neuroinflammatory markers were, however, not altered in MAGL-NKO mice (Figures S3E–S3H). MAGL-AKO mice showed an intermediate phenotype, with modest but significant reductions in LPS-induced brain cytokine and unaltered microglial activation compared to $MAGL^{+/+}$ mice (Figures S3I–S3L). Consistent with the absence of changes in bulk brain lipids in MAGL-MKO mice, these animals displayed no alterations in LPS-induced prostaglandin and cytokines production or microglial activation (Figures S4A–S4D). We did find, however, that cultured $MAGL^{-/-}$ microglia were impaired in producing prostaglandins and also displayed substantially reduced in vitro inflammatory responses (Figures S4E and S4F), consistent with recent reports (Pihlaja et al., 2015). It is possible that incomplete removal

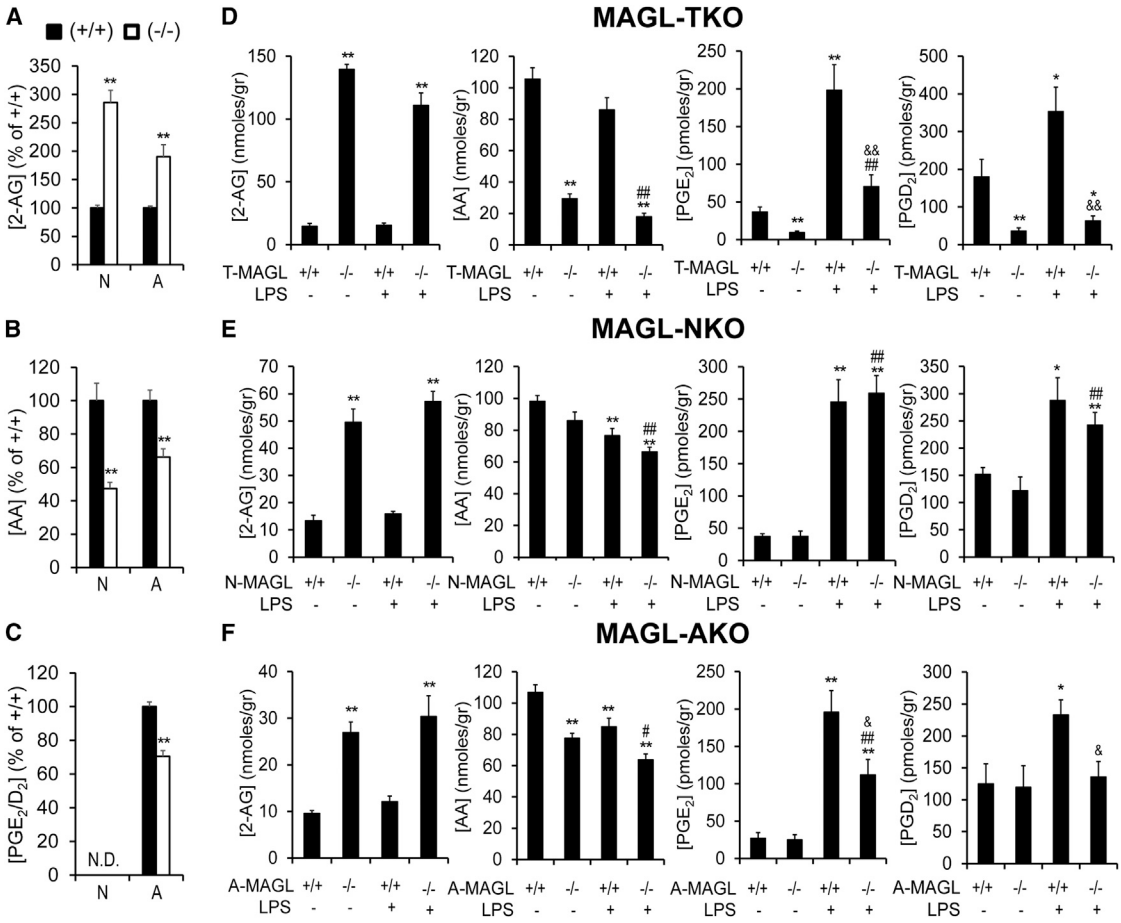

Figure 4. Astrocytes Hydrolyze 2-AG to Generate AA Precursor Pools for Pro-inflammatory Prostaglandin Production

(A–C) 2-AG (A), AA (B), and $PGDE_2/D_2$ (C) levels in $MAGL^{+/+}$ and $MAGL^{-/-}$ neurons and astrocytes. N, neurons; A, astrocytes.; N.D., not detectable. n = 5 per cell type and genotype. Error bars represent SEM; **p < 0.01 versus corresponding $MAGL^{+/+}$ cells.

(D–F) Brain levels of 2-AG, AA, PGE_2, and PGD_2 in MAGL-TKO (D), MAGL-NKO (E), and MAGL-AKO (F) mice following administration of vehicle or LPS (20 mg/kg intraperitoneally, 6 hr). n = 6–8 mice per genotype and treatment. Error bars represent SEM; *p < 0.05 and **p < 0.01 versus corresponding $MAGL^{+/+}$ vehicle treated; #p < 0.05 and ##p < 0.01 versus $MAGL^{-/-}$ vehicle treated; &p < 0.05 and &&p < 0.01 versus $MAGL^{+/+}$ LPS treated.

See also Figures S3 and S4.

of MAGL from all brain microglia in the MAGL-MKO mice (Figure S1E) prevented observation of a contribution from microglia-derived MAGL to neuroinflammatory responses in vivo.

Taken together, our in vitro and in vivo data provide strong evidence that eCB-eicosanoid crosstalk depends on the coordinated metabolic activities of neurons and astrocytes, with the former cell type providing robust production of 2-AG and the latter possessing the capacity to convert this eCB into prostaglandins. As such, robust anti-neuroinflammatory effects were only observed following global (versus cell-type-specific) deletion of MAGL, supporting a central role for neuronal-astrocytic crosstalk in the regulation of eCB-eicosanoid networks in the nervous system under pathological conditions.

Neuronal-Astrocytic Transcellular Shuttling of 2-AG and Related Metabolites

Bidirectional shuttling of conventional neurotransmitters (e.g., glutamate and GABA) and their metabolic products between neurons and glia is an established mechanism by which distinct cellular pools of these chemical messengers and their signaling activities can be regulated (Coulter and Eid, 2012). We postulated that 2-AG and/or 2-AG-derived metabolites might participate in a similar mode of intercellular transfer between neurons and astrocytes, which could provide a mechanism to rebalance bioactive lipid pools across these two cell types. To investigate this possibility, we measured 2-AG and related metabolites in $MAGL^{+/+}$ and $MAGL^{-/-}$ neurons grown by themselves or co-cultured with astrocytes in transwell dishes with polycarbonate membrane-permeable supports, which permitted free exchange of secreted metabolites in the absence of cell-cell contact. We found that, when cultured alone, $MAGL^{-/-}$ neurons accumulated and released higher amounts of 2-AG compared to $MAGL^{+/+}$ neurons and experienced a corresponding depletion in intracellular AA content (Figures 5A and 5B). In the presence of $MAGL^{+/+}$ astrocytes, however, $MAGL^{-/-}$ neurons showed smaller relative elevations in intracellular and, especially,

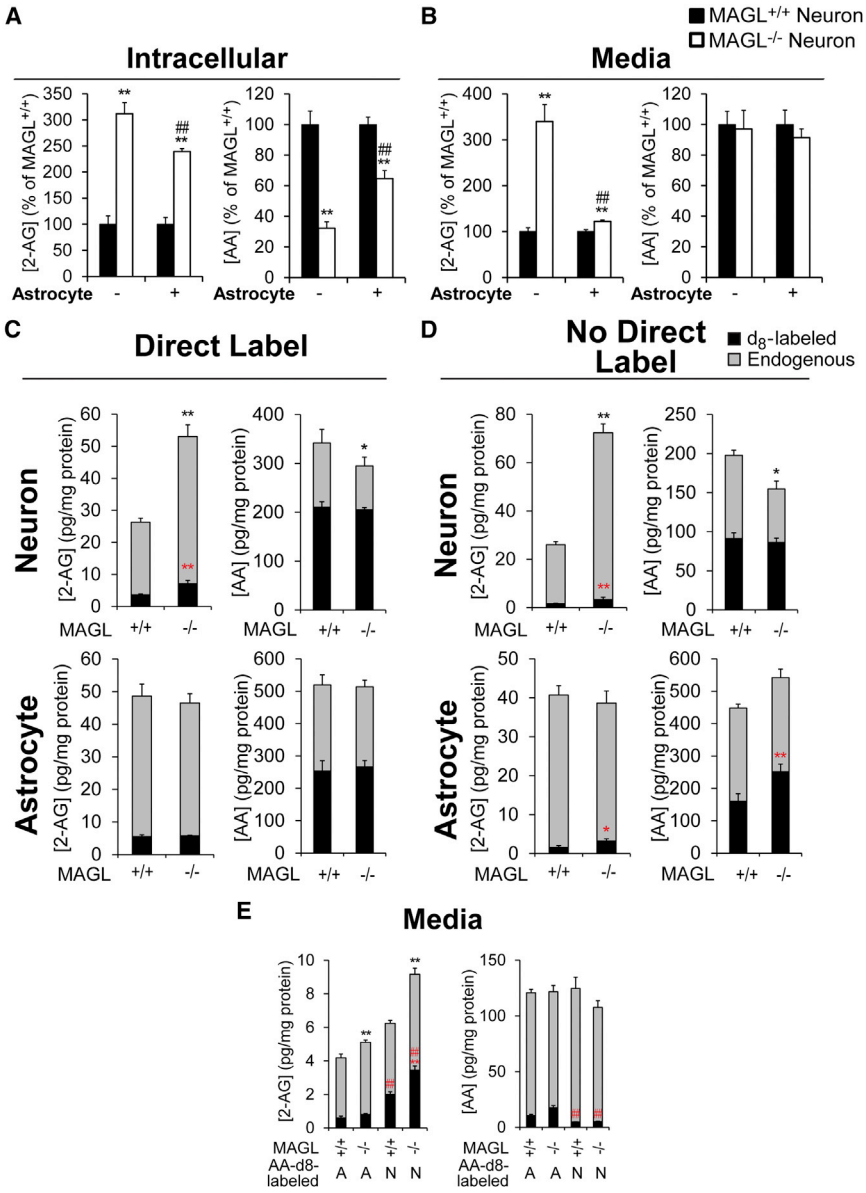

Figure 5. Transcellular Shuttling of 2-AG and AA between Neurons and Astrocytes

(A and B) Intracellular (A) and media (B) 2-AG and AA levels from MAGL$^{+/+}$ and MAGL$^{-/-}$ neurons cultured alone (–) or in the presence of astrocytes (+) in transwell co-culture dishes. n = 5 per genotype. Error bars represent SEM; **p < 0.01 versus MAGL$^{+/+}$. ##p < 0.01 versus MAGL$^{-/-}$ neurons cultured without astrocytes.

(C and D) Intracellular endogenous (gray bars) and d_8-labeled (black bars) 2-AG and AA levels from MAGL$^{+/+}$ and MAGL$^{-/-}$ neurons and MAGL$^{+/+}$ astrocytes co-cultured together for 36 hr following direct labeling of only one of the two cell types with AA-d_8. AA-d_8 is readily incorporated into intracellular lipid pools of both neurons and astrocytes (C) and is transferred to co-cultured cells that have not themselves directly received AA-d_8 (D). n = 5 per genotype. Error bars represent SEM; *p < 0.05 and **p < 0.01 versus corresponding MAGL$^{+/+}$ cells.

(E) Endogenous and d_8-labeled 2-AG and AA levels in media from MAGL$^{+/+}$ and MAGL$^{-/-}$ neurons and MAGL$^{+/+}$ astrocytes co-cultured together for 36 hr following direct AA-d_8 labeling of only one of the two cell types. n = 5 per genotype. Error bars represent SEM; **p < 0.01 versus corresponding MAGL$^{+/+}$. ##p < 0.01 versus labeled astrocytes.

secreted 2-AG, and attenuated reductions in intracellular AA content (Figures 5A and 5B). Deletion of MAGL did not affect secreted AA, although the absolute quantity of this lipid was higher in the media of neuron/astrocyte co-cultures compared to isolated neurons (neuron MAGL$^{+/+}$ = 128 ± 89; neuron MAGL$^{-/-}$ = 125 ± 12; co-culture MAGL$^{+/+}$ astrocytes/MAGL$^{+/+}$ neurons = 326 ± 19; co-culture MAGL$^{+/+}$ astrocytes/MAGL$^{-/-}$ neurons = 298 ± 43 pmol/mg protein; Figure 5B). Together, these data indicated that astrocytes can take up 2-AG released from neurons and may, in turn, deliver 2-AG-derived metabolites (e.g., AA) back to neurons.

We next used metabolic labeling methods to examine in more depth the bidirectional shuttling of AA-derived metabolites between neurons and astrocytes. AA-d_8 added to media was readily incorporated into intracellular lipids of either neurons or astrocytes in culture, including 2-AG (2AG-d_8) (Figure 5C) and other pools of neutral lipids and phospholipids (e.g., 18:0, 20:4 DAG-d_8, 18:0, 20:4 PS-d_8; d_8-labeled prostaglandins were not detected, presumably due to their low abundance; Figures S5A and S5B). AA-d_8-labeled astrocytes and neurons were then co-cultured with "naïve" neurons or astrocytes, respectively, in transwell dishes (36 hr co-culture; see Methods), which resulted in extensive incorporation of AA-d_8 in the naive cells (Figures 5D, S5C, and S5D). Examination of media from these co-cultures revealed that AA-d_8-labeled neurons released higher amounts of 2AG-d_8 compared to AA-d_8-labeled astrocytes, which preferentially secreted free AA-d_8 (Figure 5E). Of note, AA-d_8-labeled MAGL$^{-/-}$ neurons accumulated and released more 2-AG-d_8 than AA-d_8-labeled MAGL$^{+/+}$ neurons (Figures 5C and 5E), resulting in higher uptake and metabolism of this eCB by neighboring "naïve" astrocytes (Figures 5D and S5D). Even without being directly labeled with AA-d_8, MAGL$^{-/-}$ neurons also accumulated more 2-AG-d_8 than MAGL$^{+/+}$ neurons when co-cultured with AA-d_8-labeled MAGL$^{+/+}$ astrocytes (Figure 5D). These data thus provide evidence that transcellular shuttling from neurons to astrocytes contributes to the metabolism of 2-AG, and, conversely, astrocyte-derived AA can be returned to neurons to rebalance the synthesis of arachidonoyl-containing lipids, including 2-AG itself (Figure 6).

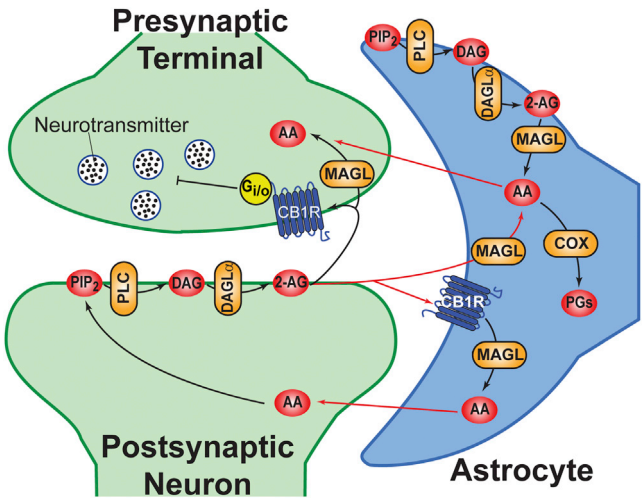

Figure 6. Distributed Oversight of 2-AG Metabolism and Function in Neurons and Astrocytes

Proposed model of astrocytic-neuronal transcellular shuttling and metabolism of 2-AG and AA. PIP2, phosphatidylinositol 4,5-biphosphate; PLC, phospholipase C; DAG, diacylglycerol; DAGLα, diacylglycerol lipase alpha; COX, cyclooxygenase.

DISCUSSION

Pharmacological or genetic disruption of MAGL produces profound changes in synaptic plasticity, neurophysiology, and behavior (Blankman and Cravatt, 2013; Murataeva et al., 2014), underscoring the substantive role played by 2-AG as a lipid transmitter in the nervous system. Considering the diverse signaling and metabolic functions of 2-AG, and that acute versus chronic blockade of MAGL often results in opposing outcomes—reflective of heightened 2-AG-mediated agonism and functional antagonism of CB_1Rs, respectively—it stands to reason that the enzymatic termination of this eCB would be spatially and temporally organized in the nervous system to guard against excess activity. One established mechanism to limit 2-AG action is the positioning of MAGL at presynaptic terminals of neurons in close proximity to CB_1Rs (Straiker et al., 2009). Whether this subcellular distribution reflects a dominant role for neurons in the control of 2-AG signaling capacity, however, remains unknown. By leveraging a mouse line that imparts conditional deletion of MAGL in specific brain cell types, we show that the metabolism of 2-AG in vivo depends on both neurons and astrocytes and that crosstalk between these cells modulates eCB-eicosanoid signaling networks to affect synaptic plasticity, neuroinflammation, and neurobehavioral processes.

Some features of 2-AG metabolism and signaling were affected to similar degrees by deletion of MAGL in neurons and astrocytes. Selective loss of MAGL in neurons or astrocytes, for instance, comparably attenuated cerebellar DSE and hippocampal DSI in comparison to MAGL-TKO mice, suggesting complementary roles for these cell types in terminating retrograde 2-AG signaling. Our findings are also consistent with a recent study showing that heterologous expression of MAGL in Bergmann glia reverses the prolonged cerebellar DSE observed in global $MAGL^{-/-}$ mice (Tanimura et al., 2012) and extend this work in an important way by determining the function of endogenously expressed astrocytic MAGL in terminating 2-AG-mediated synaptic plasticity events in different brain regions. Perhaps most strikingly, we found that selective deletion of MAGL in either neurons or astrocytes, despite producing significant elevations in brain 2-AG (5- and 3-fold, respectively), averted the CB_1R desensitization and behavioral tolerance caused by global MAGL inactivation. The distributed metabolism of 2-AG across neurons and astrocytes thus protects the nervous system from adaptive changes caused by excessive eCB signaling. In this manner, 2-AG metabolism appears to differ from the cell-type-dominant inactivation observed for more conventional neurotransmitters (e.g., astrocytes primarily inactivate glutamate, while neurons mainly terminate GABA signaling; Schousboe et al., 2013). We should further note that the relative contributions of neuronal and astrocytic MAGL to 2-AG signal termination may differ at individual synapses, as not all CB_1R-positive nerve terminals express MAGL (Uchigashima et al., 2011).

Our studies also uncovered distinct and complementary roles for neurons and astrocytes in 2-AG metabolism. MAGL deletion in neurons caused a more dramatic cellular increase in 2-AG, which was also efficiently secreted from these cells. Neurons in culture, however, exhibited no detectable capacity to convert 2-AG to prostaglandins. Similarly, MAGL-NKO mice, despite having substantially elevated brain 2-AG, did not show alterations in brain AA or prostaglandins under basal or neuroinflammatory conditions. Cultured astrocytes lacking MAGL, in contrast, coupled elevations in 2-AG with reductions in AA and prostaglandins. A similar lipid profile was observed for LPS-treated MAGL-AKO mice. These data, taken together, indicate that astrocytes play a major role in facilitating eCB-eicosanoid crosstalk in the nervous system, where they appear to convert both autonomously generated and neuronally derived 2-AG into AA and eicosanoids, especially under conditions of neuroinflammation. While our studies did not provide evidence that microglia contribute to brain eCB-eicosanoid crosstalk in vivo, it is possible that bulk tissue measurements failed to detect more anatomically or temporally restricted roles for microglia in regulating eCB-eicosanoid networks. Likewise, other 2-AG metabolic enzymes (e.g., hydrolases [ABHD6, ABHD12; Blankman et al., 2007; Marrs et al., 2010] and oxygenases [COX2; Rouzer and Marnett, 2008]), as well as distinct enzymatic pathways for generating eicosanoids (e.g., PLA2G4A) (Burke and Dennis, 2009), constitute additional potential modes for metabolic regulation of eCB-eicosanoid pathways in the brain.

How might distinct pools of 2-AG in neurons and astrocytes be coordinately regulated and balanced? Our transwell co-culture studies indicate that both 2-AG and AA can shuttle between neurons and astrocytes, with neurons being the main producers of extracellular 2-AG and astrocytes converting this eCB into AA (and presumably AA-derived metabolites) that can be returned to neurons. We therefore propose a model in which neuronal 2-AG is hydrolyzed not only at synaptic terminals but also by neighboring astrocytes, which then transfer AA back to neurons to regenerate signaling pools of 2-AG (Figure 6). The

transcellular movement of 2-AG from neurons to astrocytes may be required to couple eCB and eicosanoid pathways under basal conditions in which selective deletion of MAGL in either neurons or astrocytes did not alter brain prostaglandins. In the context of neuroinflammation, however, some of the AA generated from autonomous and/or neuronal sources of 2-AG is diverted in astrocytes for prostaglandin synthesis (Figures 6 and S5E). The transcellular movement of AA and AA-derived metabolites to facilitate eicosanoid synthesis has also been shown to occur in select peripheral systems, such as between alveolar epithelial cells and macrophages or platelets and neutrophils (Folco and Murphy, 2006). Evidence has also accumulated to support the existence of lipid-binding proteins that regulate, at least in part, the uptake, transport, and release of 2-AG and AA; however, the identities and precise contributions of these proteins remain unclear (Brash, 2001; Fowler, 2013). Determining potential protein carriers and transporters that participate in neuron-astrocyte lipid shuttling represents a fertile topic for future research. Our model further shares some organizational similarity with the glutamate-glutamine cycle, in which synaptic glutamate is taken up by astrocytes, amidated into glutamine, and transferred back to neurons for re-synthesis of glutamate (Danbolt, 2001). Thus, neuron-astrocyte crosstalk appears to be a conserved mechanism for compartmentalizing and regulating the functions of diverse synaptic modulators that include both classical neurotransmitters and retrograde lipid messengers.

EXPERIMENTAL PROCEDURES

For an extended section, see Supplemental Experimental Procedures.

Generation of Conditional MAGL$^{-/-}$ Mice

Mice carrying a *loxP*-flanked catalytic exon 4 *Mgll* allele for the conditional ablation of MAGL were generated using standard gene-targeting techniques. Homozygous MAGL^{loxP} mice were bred to Rosa26-Cre (Otto et al., 2009), Eno2-Cre (Frugier et al., 2000), GFAP-Cre (Tao et al., 2011), and LysM-Cre mice (Clausen et al., 1999) to generate MAGL-TKO, MAGL-NKO, MAGL-AKO, and MAGL-MKOs respectively.

Biochemical Studies

ABPP, substrate activity assays, and agonist-stimulated [^{35}S]GTPγS binding assays were performed as previously described (Schlosburg et al., 2010) using cell membrane homogenates from 2-month-old conditional MAGL$^{-/-}$ mice and wild-type littermates or from primary neurons, astrocytes, and microglia.

Electrophysiology

DSE at PF to PC synapses and DSI at CA1 pyramidal neuron synapses were examined in cerebellar and hippocampal slices, respectively from MAGL$^{+/+}$ or MAGL$^{-/-}$ mice from the different MAGL conditional lines as previously described (Pan et al., 2009; Zhong et al., 2011).

Behavioral Assays

Two-month-old conditional MAGL$^{-/-}$ and wild-type littermates were evaluated for cannabimimetic responses (antinociception and hypothermia) following injection with WIN55,212-2 using a cumulative dosing regimen as described elsewhere (Schlosburg et al., 2010).

Liquid Chromatography-Mass Spectrometry Metabolite Profiling

Tissue lipid levels in 2-month-old MAGL$^{+/+}$ or MAGL$^{-/-}$ mice from the different MAGL conditional lines were measured from organic-soluble brain extracts by targeted MRM methods (Nomura et al., 2011).

Transwell Co-culture Studies

Neurons and astrocytes were co-cultured in 10-cm transwell dishes with polycarbonate membrane permeable supports for 16 days prior to organic extraction of lipids from each cell type separately. For AA-d_8 labeling experiments, membrane permeable supports from 12 DIV co-cultures were temporarily transferred to a separate culture dish so that either neurons or astrocytes could be labeled with AA-d_8 conjugated to BSA (Rouzer et al., 2006). After 48 hr, cells were thoroughly washed and returned to the original co-culture for another 36 hr prior to organic extraction of lipids from each cell type separately.

SUPPLEMENTAL INFORMATION

Supplemental Information includes Supplemental Experimental Procedures, five figures, and one table and can be found with this article online at http://dx.doi.org/10.1016/j.celrep.2015.06.075.

AUTHOR CONTRIBUTIONS

A.V., J.L.B, Q.-S.L., J.E.S., D.E.S, L.J.S, A.H.L, and B.F.C. designed the experiments; A.V., J.L.B, C.M.J., P.Z., X.L., J.E.S., and A.J.T. did the experiments; A.V., J.L.B, Q.-S.L., A.J.T, and D.E.S. analyzed data; and A.V. and B.F.C. wrote the manuscript.

ACKNOWLEDGMENTS

We thank members of the Cravatt lab for helpful discussions and technical assistance. This work was supported by the NIH grants DA033760, DA032933 (B.F.C.), GM109315 (A.V.), DA037344 (J.E.S.), DA035217 and MH101146 (Q.-S.L.), and DA030404 (L.J.S. and D.E.S.). B.F.C. is a founder and scientific advisor to Abide Therapeutics, a biotechnology company interested in developing serine hydrolase inhibitors as therapeutics.

Received: January 21, 2015
Revised: June 1, 2015
Accepted: June 25, 2015
Published: July 23, 2015

REFERENCES

Allaman, I., Bélanger, M., and Magistretti, P.J. (2011). Astrocyte-neuron metabolic relationships: for better and for worse. Trends Neurosci. *34*, 76–87.

Blankman, J.L., and Cravatt, B.F. (2013). Chemical probes of endocannabinoid metabolism. Pharmacol. Rev. *65*, 849–871.

Blankman, J.L., Simon, G.M., and Cravatt, B.F. (2007). A comprehensive profile of brain enzymes that hydrolyze the endocannabinoid 2-arachidonoylglycerol. Chem. Biol. *14*, 1347–1356.

Brash, A.R. (2001). Arachidonic acid as a bioactive molecule. J. Clin. Invest. *107*, 1339–1345.

Burke, J.E., and Dennis, E.A. (2009). Phospholipase A2 structure/function, mechanism, and signaling. J. Lipid Res. *50* (*Suppl*), S237–S242.

Chanda, P.K., Gao, Y., Mark, L., Btesh, J., Strassle, B.W., Lu, P., Piesla, M.J., Zhang, M.Y., Bingham, B., Uveges, A., et al. (2010). Monoacylglycerol lipase activity is a critical modulator of the tone and integrity of the endocannabinoid system. Mol. Pharmacol. *78*, 996–1003.

Chen, R., Zhang, J., Wu, Y., Wang, D., Feng, G., Tang, Y.P., Teng, Z., and Chen, C. (2012). Monoacylglycerol lipase is a therapeutic target for Alzheimer's disease. Cell Rep. *2*, 1329–1339.

Clausen, B.E., Burkhardt, C., Reith, W., Renkawitz, R., and Förster, I. (1999). Conditional gene targeting in macrophages and granulocytes using LysMcre mice. Transgenic Res. *8*, 265–277.

Coulter, D.A., and Eid, T. (2012). Astrocytic regulation of glutamate homeostasis in epilepsy. Glia *60*, 1215–1226.

Cravatt, B.F., Giang, D.K., Mayfield, S.P., Boger, D.L., Lerner, R.A., and Gilula, N.B. (1996). Molecular characterization of an enzyme that degrades neuromodulatory fatty-acid amides. Nature *384*, 83–87.

Cravatt, B.F., Wright, A.T., and Kozarich, J.W. (2008). Activity-based protein profiling: from enzyme chemistry to proteomic chemistry. Annu. Rev. Biochem. *77*, 383–414.

Danbolt, N.C. (2001). Glutamate uptake. Prog. Neurobiol. *65*, 1–105.

Di Marzo, V., Stella, N., and Zimmer, A. (2015). Endocannabinoid signalling and the deteriorating brain. Nat. Rev. Neurosci. *16*, 30–42.

Dinh, T.P., Carpenter, D., Leslie, F.M., Freund, T.F., Katona, I., Sensi, S.L., Kathuria, S., and Piomelli, D. (2002). Brain monoglyceride lipase participating in endocannabinoid inactivation. Proc. Natl. Acad. Sci. USA *99*, 10819–10824.

Folco, G., and Murphy, R.C. (2006). Eicosanoid transcellular biosynthesis: from cell-cell interactions to in vivo tissue responses. Pharmacol. Rev. *58*, 375–388.

Fowler, C.J. (2013). Transport of endocannabinoids across the plasma membrane and within the cell. FEBS J. *280*, 1895–1904.

Fowler, C.J., Holt, S., Nilsson, O., Jonsson, K.O., Tiger, G., and Jacobsson, S.O. (2005). The endocannabinoid signaling system: pharmacological and therapeutic aspects. Pharmacol. Biochem. Behav. *81*, 248–262.

Frugier, T., Tiziano, F.D., Cifuentes-Diaz, C., Miniou, P., Roblot, N., Dierich, A., Le Meur, M., and Melki, J. (2000). Nuclear targeting defect of SMN lacking the C-terminus in a mouse model of spinal muscular atrophy. Hum. Mol. Genet. *9*, 849–858.

Halassa, M.M., and Haydon, P.G. (2010). Integrated brain circuits: astrocytic networks modulate neuronal activity and behavior. Annu. Rev. Physiol. *72*, 335–355.

Hewett, S.J., Uliasz, T.F., Vidwans, A.S., and Hewett, J.A. (2000). Cyclooxygenase-2 contributes to N-methyl-D-aspartate-mediated neuronal cell death in primary cortical cell culture. J. Pharmacol. Exp. Ther. *293*, 417–425.

Ikeda-Matsuo, Y., Ikegaya, Y., Matsuki, N., Uematsu, S., Akira, S., and Sasaki, Y. (2005). Microglia-specific expression of microsomal prostaglandin E2 synthase-1 contributes to lipopolysaccharide-induced prostaglandin E2 production. J. Neurochem. *94*, 1546–1558.

Kano, M., Ohno-Shosaku, T., Hashimotodani, Y., Uchigashima, M., and Watanabe, M. (2009). Endocannabinoid-mediated control of synaptic transmission. Physiol. Rev. *89*, 309–380.

Long, J.Z., Li, W., Booker, L., Burston, J.J., Kinsey, S.G., Schlosburg, J.E., Pavón, F.J., Serrano, A.M., Selley, D.E., Parsons, L.H., et al. (2009). Selective blockade of 2-arachidonoylglycerol hydrolysis produces cannabinoid behavioral effects. Nat. Chem. Biol. *5*, 37–44.

Marrs, W.R., Blankman, J.L., Horne, E.A., Thomazeau, A., Lin, Y.H., Coy, J., Bodor, A.L., Muccioli, G.G., Hu, S.S., Woodruff, G., et al. (2010). The serine hydrolase ABHD6 controls the accumulation and efficacy of 2-AG at cannabinoid receptors. Nat. Neurosci. *13*, 951–957.

McIver, S., Faideau, M., and Haydon, P. (2013). Astrocyte–neuron communications. In Neural-Immune Interactions in Brain Function and Alcohol Related Disorders, C. Cui, L. Grandison, and A. Noronha, eds. (Springer), pp. 31–64.

Mechoulam, R., and Hanus, L. (2000). A historical overview of chemical research on cannabinoids. Chem. Phys. Lipids *108*, 1–13.

Murataeva, N., Straiker, A., and Mackie, K. (2014). Parsing the players: 2-arachidonoylglycerol synthesis and degradation in the CNS. Br. J. Pharmacol. *171*, 1379–1391.

Navarrete, M., and Araque, A. (2008). Endocannabinoids mediate neuron-astrocyte communication. Neuron *57*, 883–893.

Navarrete, M., and Araque, A. (2010). Endocannabinoids potentiate synaptic transmission through stimulation of astrocytes. Neuron *68*, 113–126.

Nomura, D.K., Morrison, B.E., Blankman, J.L., Long, J.Z., Kinsey, S.G., Marcondes, M.C., Ward, A.M., Hahn, Y.K., Lichtman, A.H., Conti, B., and Cravatt, B.F. (2011). Endocannabinoid hydrolysis generates brain prostaglandins that promote neuroinflammation. Science *334*, 809–813.

Otto, C., Fuchs, I., Kauselmann, G., Kern, H., Zevnik, B., Andreasen, P., Schwarz, G., Altmann, H., Klewer, M., Schoor, M., et al. (2009). GPR30 does not mediate estrogenic responses in reproductive organs in mice. Biol. Reprod. *80*, 34–41.

Pacher, P., Bátkai, S., and Kunos, G. (2006). The endocannabinoid system as an emerging target of pharmacotherapy. Pharmacol. Rev. *58*, 389–462.

Pan, B., Wang, W., Long, J.Z., Sun, D., Hillard, C.J., Cravatt, B.F., and Liu, Q.S. (2009). Blockade of 2-arachidonoylglycerol hydrolysis by selective monoacylglycerol lipase inhibitor 4-nitrophenyl 4-(dibenzo[d][1,3]dioxol-5-yl(hydroxy) methyl)piperidine-1-carboxylate (JZL184) Enhances retrograde endocannabinoid signaling. J. Pharmacol. Exp. Ther. *331*, 591–597.

Pan, B., Wang, W., Zhong, P., Blankman, J.L., Cravatt, B.F., and Liu, Q.S. (2011). Alterations of endocannabinoid signaling, synaptic plasticity, learning, and memory in monoacylglycerol lipase knock-out mice. J. Neurosci. *31*, 13420–13430.

Pihlaja, R., Takkinen, J., Eskola, O., Vasara, J., López-Picón, F.R., Haaparanta-Solin, M., and Rinne, J.O. (2015). Monoacylglycerol lipase inhibitor JZL184 reduces neuroinflammatory response in APdE9 mice and in adult mouse glial cells. J. Neuroinflammation *12*, 81.

Piro, J.R., Benjamin, D.I., Duerr, J.M., Pi, Y., Gonzales, C., Wood, K.M., Schwartz, J.W., Nomura, D.K., and Samad, T.A. (2012). A dysregulated endocannabinoid-eicosanoid network supports pathogenesis in a mouse model of Alzheimer's disease. Cell Rep. *1*, 617–623.

Reisenberg, M., Singh, P.K., Williams, G., and Doherty, P. (2012). The diacylglycerol lipases: structure, regulation and roles in and beyond endocannabinoid signalling. Philos. Trans. R. Soc. Lond. B Biol. Sci. *367*, 3264–3275.

Rouzer, C.A., and Marnett, L.J. (2008). Non-redundant functions of cyclooxygenases: oxygenation of endocannabinoids. J. Biol. Chem. *283*, 8065–8069.

Rouzer, C.A., Ivanova, P.T., Byrne, M.O., Milne, S.B., Marnett, L.J., and Brown, H.A. (2006). Lipid profiling reveals arachidonate deficiency in RAW264.7 cells: Structural and functional implications. Biochemistry *45*, 14795–14808.

Salter, M.W., and Beggs, S. (2014). Sublime microglia: expanding roles for the guardians of the CNS. Cell *158*, 15–24.

Schafer, D.P., Lehrman, E.K., Kautzman, A.G., Koyama, R., Mardinly, A.R., Yamasaki, R., Ransohoff, R.M., Greenberg, M.E., Barres, B.A., and Stevens, B. (2012). Microglia sculpt postnatal neural circuits in an activity and complement-dependent manner. Neuron *74*, 691–705.

Schlosburg, J.E., Blankman, J.L., Long, J.Z., Nomura, D.K., Pan, B., Kinsey, S.G., Nguyen, P.T., Ramesh, D., Booker, L., Burston, J.J., et al. (2010). Chronic monoacylglycerol lipase blockade causes functional antagonism of the endocannabinoid system. Nat. Neurosci. *13*, 1113–1119.

Schousboe, A., Bak, L.K., and Waagepetersen, H.S. (2013). Astrocytic control of biosynthesis and turnover of the neurotransmitters glutamate and GABA. Front. Endocrinol. (Lausanne) *4*, 102.

Stella, N. (2010). Cannabinoid and cannabinoid-like receptors in microglia, astrocytes, and astrocytomas. Glia *58*, 1017–1030.

Straiker, A., Hu, S.S., Long, J.Z., Arnold, A., Wager-Miller, J., Cravatt, B.F., and Mackie, K. (2009). Monoacylglycerol lipase limits the duration of endocannabinoid-mediated depolarization-induced suppression of excitation in autaptic hippocampal neurons. Mol. Pharmacol. *76*, 1220–1227.

Tanimura, A., Uchigashima, M., Yamazaki, M., Uesaka, N., Mikuni, T., Abe, M., Hashimoto, K., Watanabe, M., Sakimura, K., and Kano, M. (2012). Synapse type-independent degradation of the endocannabinoid 2-arachidonoylglycerol after retrograde synaptic suppression. Proc. Natl. Acad. Sci. USA *109*, 12195–12200.

Tao, J., Wu, H., Lin, Q., Wei, W., Lu, X.H., Cantle, J.P., Ao, Y., Olsen, R.W., Yang, X.W., Mody, I., et al. (2011). Deletion of astroglial Dicer causes non-cell-autonomous neuronal dysfunction and degeneration. J. Neurosci. *31*, 8306–8319.

Uchigashima, M., Yamazaki, M., Yamasaki, M., Tanimura, A., Sakimura, K., Kano, M., and Watanabe, M. (2011). Molecular and morphological configuration for 2-arachidonoylglycerol-mediated retrograde signaling at mossy cell-granule cell synapses in the dentate gyrus. J. Neurosci. *31*, 7700–7714.

Ueda, N., Tsuboi, K., and Uyama, T. (2013). Metabolism of endocannabinoids and related N-acylethanolamines: canonical and alternative pathways. FEBS J. *280*, 1874–1894.

Walter, L., Dinh, T., and Stella, N. (2004). ATP induces a rapid and pronounced increase in 2-arachidonoylglycerol production by astrocytes, a response limited by monoacylglycerol lipase. J. Neurosci. *24*, 8068–8074.

Witting, A., Walter, L., Wacker, J., Möller, T., and Stella, N. (2004). P2X7 receptors control 2-arachidonoylglycerol production by microglial cells. Proc. Natl. Acad. Sci. USA *101*, 3214–3219.

Zhong, P., Pan, B., Gao, X.P., Blankman, J.L., Cravatt, B.F., and Liu, Q.S. (2011). Genetic deletion of monoacylglycerol lipase alters endocannabinoid-mediated retrograde synaptic depression in the cerebellum. J. Physiol. *589*, 4847–4855.

Cell Reports

Supplemental Information

Metabolic Interplay between Astrocytes and Neurons Regulates Endocannabinoid Action

Andreu Viader, Jacqueline L. Blankman, Peng Zhong, Xiaojie Liu, Joel E. Schlosburg, Christopher M. Joslyn, Qing-Song Liu, Aaron J. Tomarchio, Aron H. Lichtman, Dana E. Selley, Laura J. Sim-Selley, and Benjamin F. Cravatt

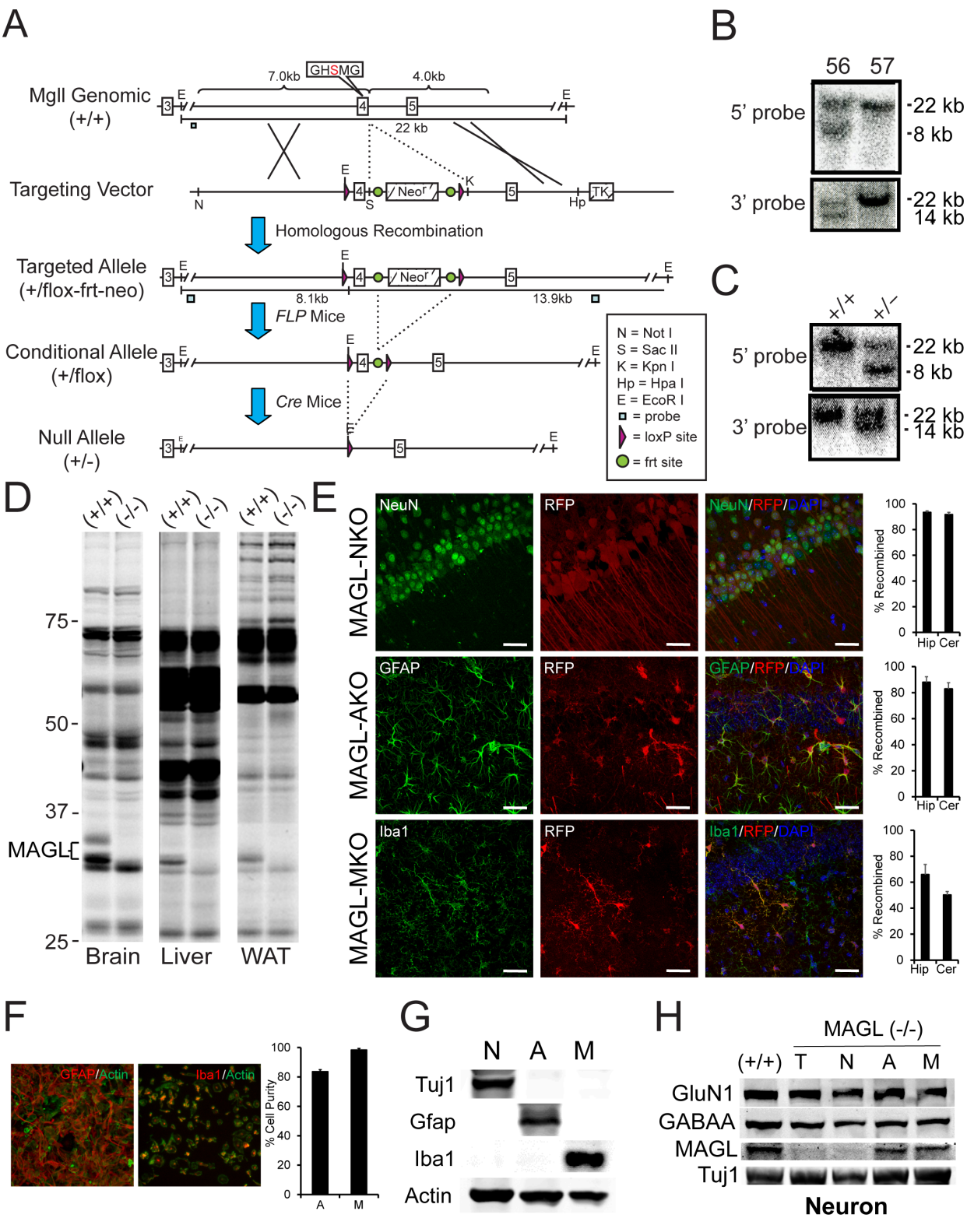
A
Mgll Genomic
(+/+)
7.0kb
GHSMG
4.0kb
22 kb
Targeting Vector
Neo
TK
Homologous Recombination
Targeted Allele
(+/flox-frt-neo)
8.1kb
13.9kb
FLP Mice
Conditional Allele
(+/flox)
Cre Mice
Null Allele
(+/-)
N = Not I
S = Sac II
K = Kpn I
Hp = Hpa I
E = EcoR I
= probe
= loxP site
= frt site
B
56 57
5' probe
3' probe
22 kb
8 kb
22 kb
14 kb
C
5' probe
3' probe
22 kb
8 kb
22 kb
14 kb
D
75
50
37
MAGL
25
Brain
Liver
WAT
E
MAGL-NKO
MAGL-AKO
MAGL-MKO
NeuN
GFAP
Iba1
RFP
NeuN/RFP/DAPI
GFAP/RFP/DAPI
Iba1/RFP/DAPI
% Recombined
Hip Cer
F
GFAP/Actin
Iba1/Actin
% Cell Purity
A
M
G
N A M
Tuj1
Gfap
Iba1
Actin
H
MAGL (-/-)
(+/+) T N A M
GluN1
GABAA
MAGL
Tuj1
Neuron

Figure S1, related to Figure 1. Generation and characterization of conditional MAGL$^{-/-}$ mice.

(A) Targeting vector used to flank *Mgll* exon 4 (containing catalytic S122) with *loxP* recombination sites to enable conditional *Cre* recombinase-mediated gene deletion.

(B) Identification of targeted clone no. 56 by Southern analysis of *EcoRI*-digested ES cell genomic DNA with external 5' and 3' probes.

(C) Southern analysis confirmation of germ-line transmission in a chimeric male arising from injection of clone no.56 into albino C57BL/6 blastocysts.

(D) Activity-based protein profiling of brain, liver, and white adipose tissue (WAT) membrane proteomes from MAGL-TKO mice and wild-type littermates confirms global loss of MAGL across different tissues in the MAGL-TKO animals.

(E) Representative confocal images of brain sections from Rosa26-tdTomato/Eno2-Cre (MAGL-NKO), GFAP-Cre (MAGL-AKO), and LysM-cre (MAGL-MKO) mice co-stained for reporter protein tdTomato (RFP) and neuronal (NeuN), astroglial (GFAP) and microglial (Iba1) markers, confirm efficient, widespread, but largely cell-selective cre-mediated recombination. Quantification of % recombination of hippocampal (Hip) and cerebellar (Cer) neurons, astrocytes, and microglia in Rosa26-tdTomato/Eno2-Cre, GFAP-Cre, and LysM-cre mice respectively is shown. Note that, as previously reported (Tao et al., 2011), 2-6% of neurons in Rosa26-tdTomato/GFAP-Cre mice show cre-mediated recombination. Scale bars 30 μm. N=2 mice per genotype.

(F, G) Immunocytochemical (F) and western blot (G) analysis of neuron, astrocyte and microglia cultures with cell type-specific markers (Tuj1, GFAP, and Iba1 respectively; actin used to visualized all cells), confirms high degree of enrichment of cultures used to

examine MAGL deletion in these cell types. (H) Western blot of neurons derived from MAGL-TKO (T), -NKO (N), -AKO (A), or –MKO (M) mice shows that these cultures include both glutamatergic (glutamate receptor-expressing neurons, GluN1/NR1) and GABAergic neurons (GABA receptor-expressing neurons, GABAA α1), and that MAGL is ablated in both neuron types specifically in MAGL-TKO and -NKO mice.

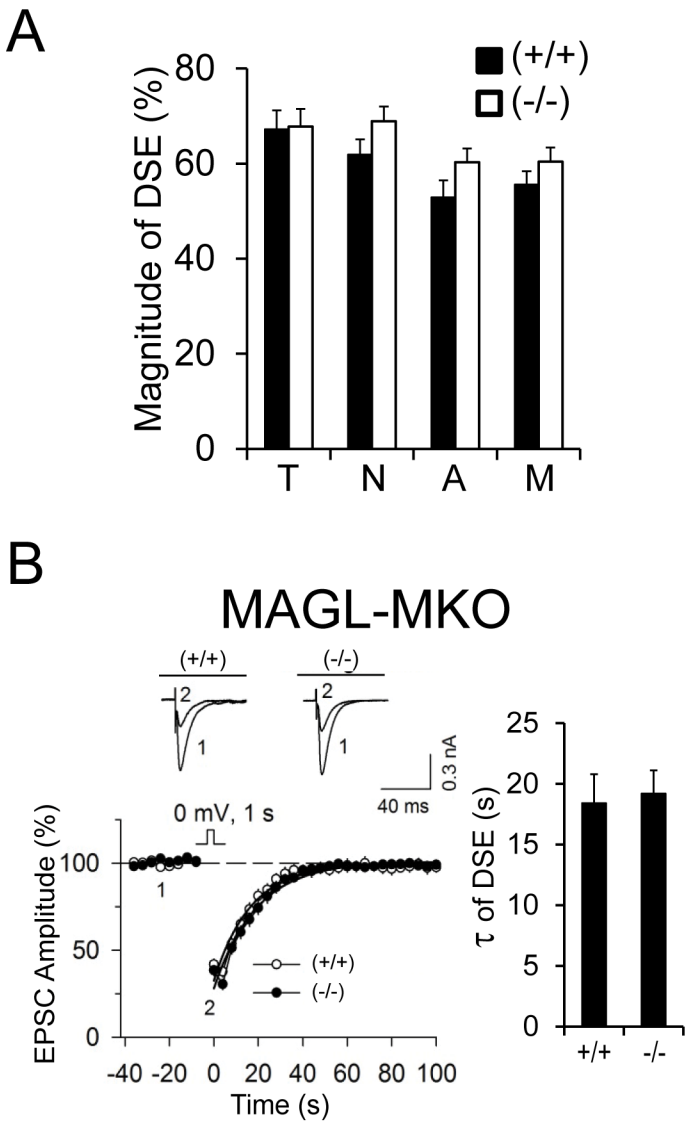

Figure S2, related to Figure 2. Characterization of DSE properties in cerebellar slices from MAGL-disrupted mouse models.

(A) Magnitude of DSE in cerebellar slices prepared from MAGL-TKO (T), -NKO (N), -AKO (A), and –MKO (M) mice and their wild-type littermates. n=14-18 cells from N=3 mice per genotype. Error bars represent SEM.

(B) Sample traces (top), average time courses (bottom) and decay time constant (τ, right) of PF-EPSCs in cerebellar slices prepared from MAGL-MKO mice. n=14-18 cells from N=3 mice per genotype. Error bars represent SEM.

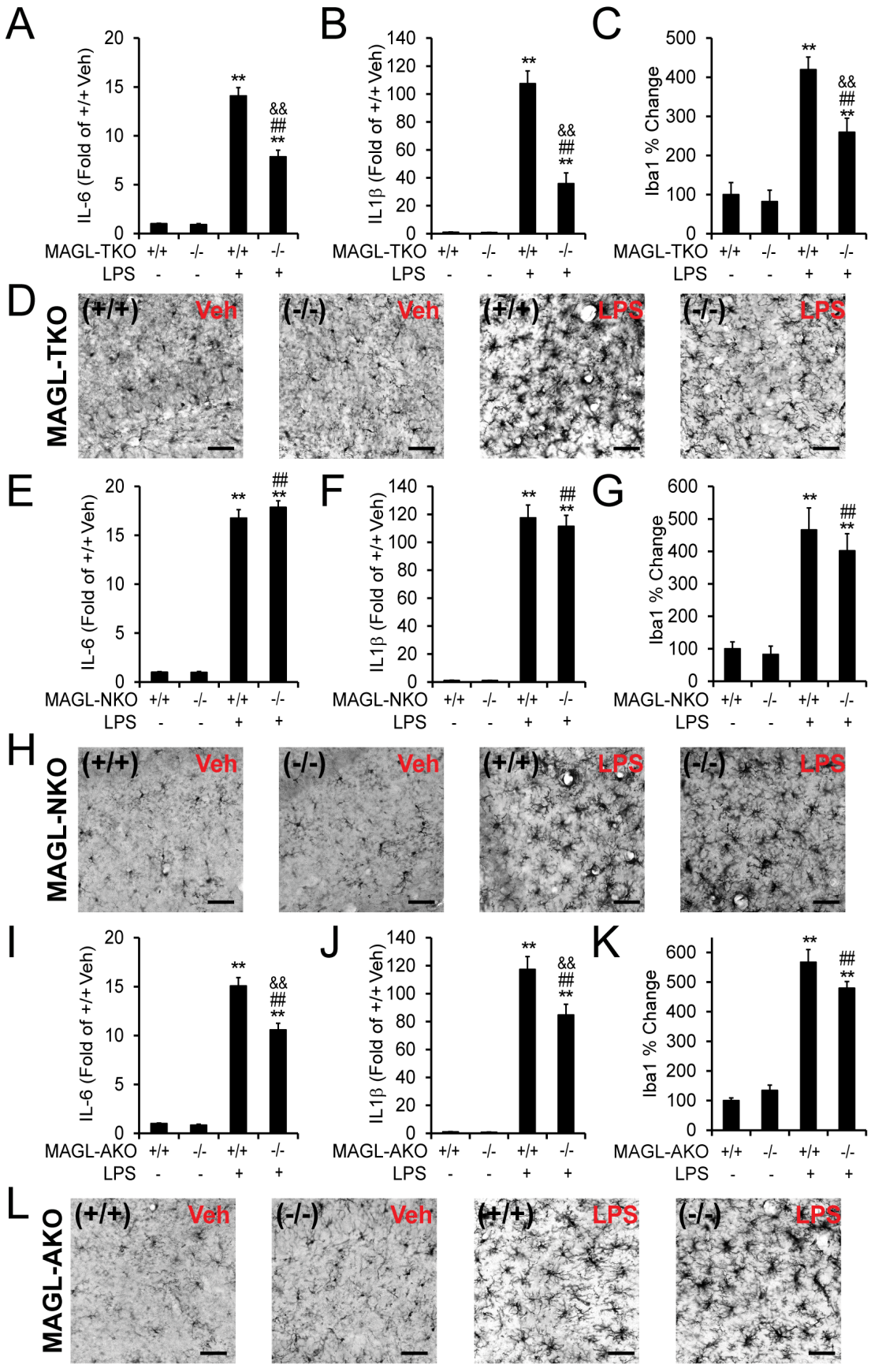
A
IL-6 (Fold of +/+ Veh)
MAGL-TKO +/+ -/- +/+ -/-
LPS - - + +
B
IL1β (Fold of +/+ Veh)
MAGL-TKO +/+ -/- +/+ -/-
LPS - - + +
C
Iba1 % Change
MAGL-TKO +/+ -/- +/+ -/-
LPS - - + +
D
MAGL-TKO
(+/+) Veh
(-/-) Veh
(+/+) LPS
(-/-) LPS
E
IL-6 (Fold of +/+ Veh)
MAGL-NKO +/+ -/- +/+ -/-
LPS - - + +
F
IL1β (Fold of +/+ Veh)
MAGL-NKO +/+ -/- +/+ -/-
LPS - - + +
G
Iba1 % Change
MAGL-NKO +/+ -/- +/+ -/-
LPS - - + +
H
MAGL-NKO
(+/+) Veh
(-/-) Veh
(+/+) LPS
(-/-) LPS
I
IL-6 (Fold of +/+ Veh)
MAGL-AKO +/+ -/- +/+ -/-
LPS - - + +
J
IL1β (Fold of +/+ Veh)
MAGL-AKO +/+ -/- +/+ -/-
LPS - - + +
K
Iba1 % Change
MAGL-AKO +/+ -/- +/+ -/-
LPS - - + +
L
MAGL-AKO
(+/+) Veh
(-/-) Veh
(+/+) LPS
(-/-) LPS

Figure S3, related to Figure 4. Astrocyte- but not neuron-specific loss of MAGL attenuates neuroinflammatory responses in mice.

(A, B; E, F; I, J) Inflammatory cytokine levels as measured by ELISA in brains from MAGL-TKO (A, B), MAGL-NKO (E, F), or MAGL-AKO (I, J) mice and corresponding wild-type littermates following administration of vehicle or LPS (20 mg/kg, i.p., 6 hours). N=6-8 per treatment and genotype. Error bars represent SEM; **p<0.01 vs. $MAGL^{+/+}$ vehicle-treated; ##p<0.01 vs. $MAGL^{-/-}$ vehicle-treated; &&p<0.01 vs. $MAGL^{+/+}$ LPS-treated.

(C, D; G, H; K, L) Quantification and representative pictures of microglial activation assessed by Iba-1 staining in hippocampal regions from MAGL-TKO (C, D), MAGL-NKO (G, H), or MAGL-AKO (K, L) and corresponding wild-type littermates following administration of vehicle or LPS (1 mg/kg once per day for 4 days). Scale bar, 50 μm. N=5 per treatment and genotype. Error bars represent SEM; **p<0.01 vs. $MAGL^{+/+}$ vehicle-treated; ##p<0.01 vs. $MAGL^{-/-}$ vehicle-treated; &&p<0.01 vs. $MAGL^{+/+}$ LPS-treated.

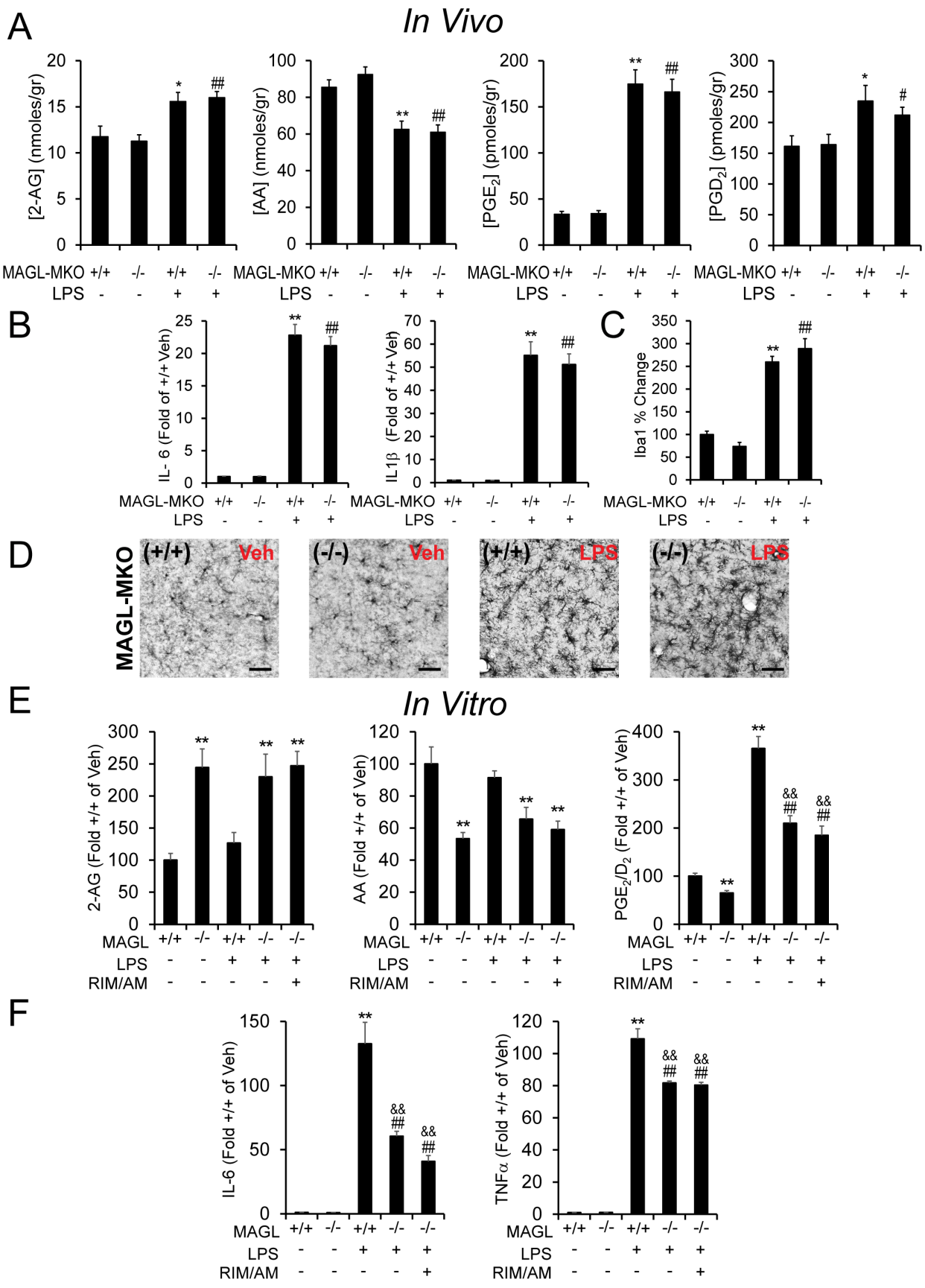
A
In Vivo
[2-AG] (nmoles/gr)
[AA] (nmoles/gr)
[PGE2] (pmoles/gr)
[PGD2] (pmoles/gr)
MAGL-MKO +/+ -/- +/+ -/-
LPS - - + +
B
IL- 6 (Fold of +/+ Veh)
IL1β (Fold of +/+ Veh)
C
Iba1 % Change
D
MAGL-MKO
(+/+) Veh
(-/-) Veh
(+/+) LPS
(-/-) LPS
E
In Vitro
2-AG (Fold +/+ of Veh)
AA (Fold +/+ of Veh)
PGE2/D2 (Fold +/+ of Veh)
MAGL +/+ -/- +/+ -/- -/-
LPS - - + + +
RIM/AM - - - - +
F
IL-6 (Fold +/+ of Veh)
TNFα (Fold +/+ of Veh)

Figure S4, related to Figure 4. Microglia-specific loss of MAGL attenuates inflammatory responses *in vitro,* but does not *in vivo.*

(A) Brain levels of 2-AG, AA, PGE_2, and PGD_2 in MAGL-MKO mice following administration of vehicle or LPS (20 mg/kg, i.p., 6 hours). N=6-8 mice per genotype and treatment. Error bars represent SEM; *p<0.05 and **p<0.01 vs. $MAGL^{+/+}$ vehicle-treated; #p<0.05 and ##p<0.01 vs. $MAGL^{-/-}$ vehicle-treated.

(B) Inflammatory cytokine levels as measured by ELISA in brains from MAGL-MKO mice and corresponding wild-type littermates following administration of vehicle or LPS (20 mg/kg, i.p., 6 hours). N=6-8 per treatment and genotype. Error bars represent SEM; **p<0.01 vs. $MAGL^{+/+}$ vehicle-treated; ##p<0.01 vs. $MAGL^{-/-}$ vehicle-treated.

(C, D) Quantification (C) and representative pictures (D) of microglial activation assessed by Iba-1 staining in hippocampal regions from MAGL-MKO mice and corresponding wild-type littermates following administration of vehicle or LPS (1 mg/kg once per day for 4 days). Scale bar, 50 μm. N=5 per treatment and genotype. Error bars represent SEM; **p<0.01 vs. $MAGL^{+/+}$ vehicle-treated; ##p<0.01 vs. $MAGL^{-/-}$ vehicle-treated; &&p<0.01 vs. $MAGL^{+/+}$ LPS-treated.

(E) Levels of 2-AG, AA, and PGE_2/D_2 basally as well as after exposure to the pro-inflammatory agent lipopolysaccharide (LPS; 100 ng/mL for 4 hours) in $MAGL^{+/+}$ and $MAGL^{-/-}$ microglia. Note that pre-treatment with $CB_{1/2}R$ inhibitors rimonabant and AM630, respectively (5 μM each, 1 h pre-treatment), did not block MAGL deletion-induced reduction in LPS-induced prostaglandin synthesis. N=5 per genotype and treatment. Error bars represent SEM; **p<0.01 vs. $MAGL^{+/+}$ vehicle-treated; ##p<0.01 vs. $MAGL^{-/-}$ vehicle-treated; &&p<0.01 vs. $MAGL^{+/+}$ LPS-treated.

(F) LPS-induced (100 ng/mL for 4 hours) inflammatory cytokine levels as measured by ELISA in $MAGL^{+/+}$ and $MAGL^{-/-}$ microglia. Note that pre-treatment with $CB_{1/2}R$ inhibitors rimonabant and AM630, respectively (5 μM each, 1 h pre-treatment), did not block MAGL deletion-induced reduction in LPS-induced cytokine production. N=5 per genotype and treatment. Error bars represent SEM; **p<0.01 vs. $MAGL^{+/+}$ vehicle-treated; ##p<0.01 vs. $MAGL^{-/-}$ vehicle-treated; &&p<0.01 vs. $MAGL^{+/+}$ LPS-treated.

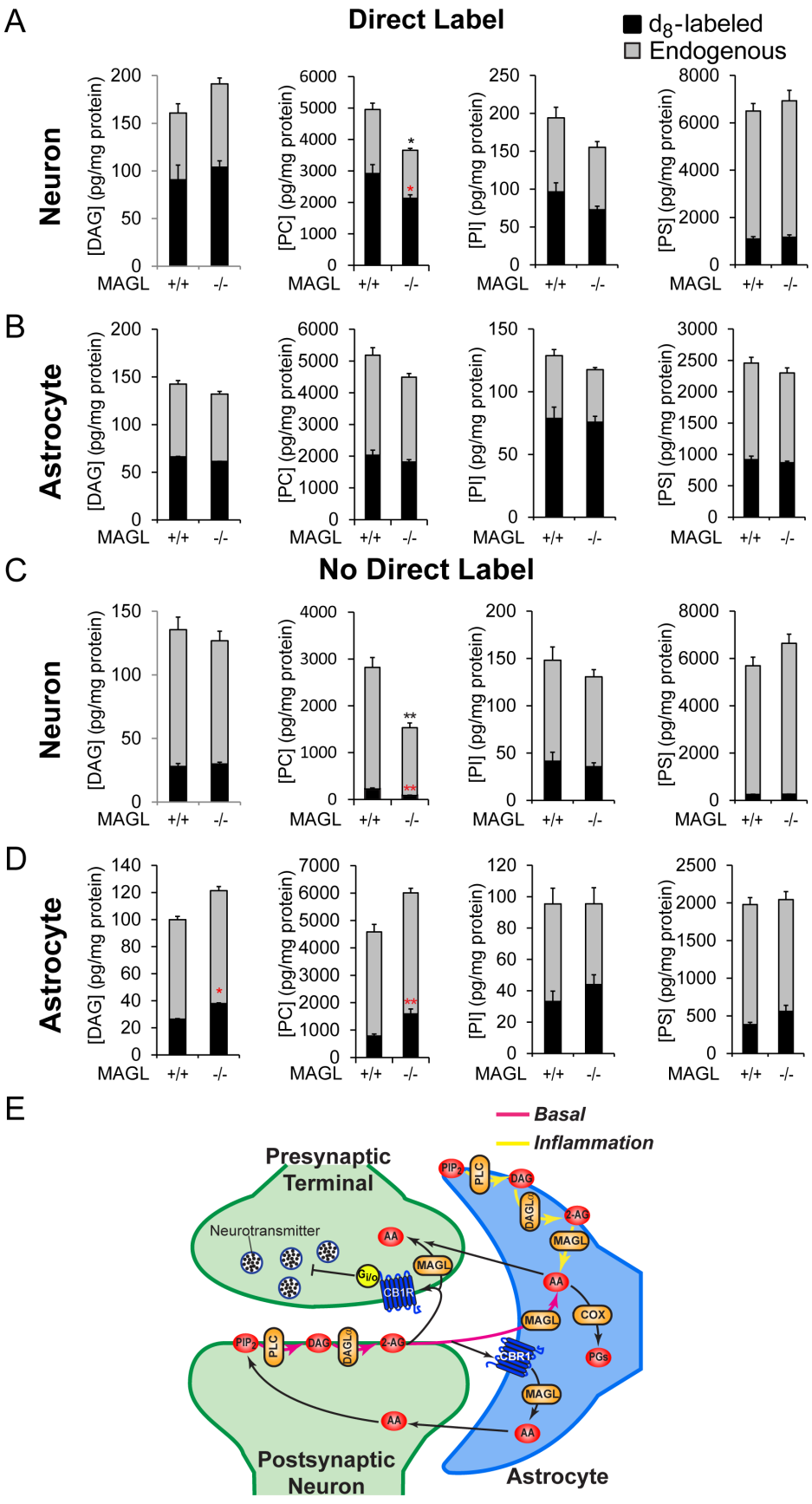
A
Direct Label
d8-labeled
Endogenous
Neuron
[DAG] (pg/mg protein)
[PC] (pg/mg protein)
[PI] (pg/mg protein)
[PS] (pg/mg protein)
MAGL +/+ -/-
B
Astrocyte
C
No Direct Label
D
E
Basal
Inflammation
Presynaptic Terminal
Neurotransmitter
AA
MAGL
Gi/o
CB1R
PIP2
PLC
DAG
DAGL
2-AG
COX
PGs
CBR1?
Postsynaptic Neuron
Astrocyte

Figure S5, related to Figure 5 and 6. Transcellular shuttling of arachidonate metabolites between neurons and astrocytes.

(A-D) Intracellular levels of endogenous (gray bars) and d_8-labeled (black bars) AA-containing lipids in $MAGL^{+/+}$ and $MAGL^{-/-}$ neurons and $MAGL^{+/+}$ astrocytes co-cultured together for 36 h following direct labeling of only one of the two cell types with AA-d_8. AA-d_8 is readily incorporated into intracellular lipid pools of both neurons and astrocytes (A, B) and is transferred to co-cultured cells that have not themselves directly received AA-d_8 (C, D). DAG, diacylglycerol, C18:0/C20:4; PC, phosphatidylcholine C18:0/C20:4; PI, phosphatidylinositol C18:0/C20:4; PS, phosphatidylserine C18:0/C20:4. N=5 per genotype. Error bars represent SEM; *$p < 0.05$ and **$p < 0.01$ vs. $MAGL^{+/+}$ cells.

(H) Proposed model for how astrocytic-neuronal transcellular metabolism regulates eCB-eicosanoid crosstalk under basal and neuroinflammatory conditions. In basal conditions, hydrolysis of neuron-derived 2-AG in astrocytes provides a principal source for prostaglandin production (pink arrows), such that reductions in basal prostaglandins requires deletion of MAGL in both neurons and astrocytes. Following exposure to inflammatory stimuli, 2-AG autonomously generated in astrocytes becomes a major source of AA for prostaglandin synthesis (yellow arrows); hence, in states of neuroinflammation (e.g., LPS-treatment), reductions in brain prostaglandins are observed in mice with global or astrocyte-specific loss of MAGL.

Supplemental Experimental Procedures

Materials. Fluorophosphonate (FP)-rhodamine was synthesized as previously described (Patricelli et al., 2001). All deuterated lipid standards and substrates were purchased from Cayman Chemicals. Lipopolysaccharide from *E. coli* was purchased from Sigma (0111:B4).

Generation of MAGL^{loxP} mice, matings and genotyping. All animal experiments were carried out in compliance with institutional animal protocols, and mice were housed on a normal 6AM/6PM light/dark phase with ad libitum access to water and food. A MAGL conditional knockout construct targeting the deletion of *Mgll* catalytic exon 4 was generated by amplifying 7 and 4 kb regions of the *Mgll* gene adjacent to the catalytic exon 4 from a BAC clone containing the *Mgll* locus (clone ID RP23-82I13, BACPAC Resources, Children's Hospital Oakland Research Institute) and subcloning these homologous arms into the NotI/SacII and KpnI/HpaI sites of the pKO12 vector. This targeting construct consisted of exon 4 flanked by *loxP* sites (for future excision by the *Cre* recombinase), a flrted neomycin cassette (for the positive selection of integrated clones following treatment with geneticin), and homologous arms of genomic DNA at either side (to target the construct to the genomic locus). A thymidine kinase gene-cassette was also included just outside the homologous arms to serve as a ganciclovir-sensitive negative selection marker against clones in which the constructs had integrated by non-homologous recombination. Following electroporation of the targeting construct in C57BL/6 Bruce 4-derived murine embryonic stem (ES) cells, ~3000 integrated ES cell clones were obtained and screened for homologous recombination by Southern blot analysis with external probes located 5' and 3' of the targeted region. These probes gave differential band sizes in wild-type (22 kb) or targeted (5' probe, 8.1

kb; 3' probe, 13.9 kb) genomic DNA digested with EcoRI. One homologous recombinant, 56, was identified, expanded and injected into albino C57BL/6 blastocysts. Blastocyst implantation into pseudopregnant albino C57BL/6 females generated six chimeric males, two of which gave rise to germline transmission as determined by coat color and Southern analysis. These mice were bred to homozygocity to produce MAGL^{loxP} mice *(Mgll$^{loxP/loxP)}$*. MAGL-TKOs (*Mgll$^{-/-}$*) and control littermates (*Mgll$^{+/+}$*) were generated by crossing *Mgll$^{loxP/loxP}$* mice to Rosa26-Cre mice (Taconic model #12524) (Otto et al., 2009), backcrossing the resulting offspring heterozygous for the null allele with C57BL/6 mice to eliminate the *Cre* recombinase transgene, and then setting up heterozygous matings. MAGL-NKO, -AKO, and –MKO mice were generated by crossing *Mgll$^{loxP/loxP}$* to Eno2-Cre (Jax stock #005938) (Frugier et al., 2000), GFAP-Cre (Jax stock #012887) (Tao et al., 2011) and LysM-Cre (Jax stock #004781) (Clausen et al., 1999) mice respectively, then backcrossing the resulting double heterozygotes (*Cre$^{+/-}$*, *Mgll$^{+/loxP}$*) to *Mgll$^{loxP/loxP}$* to produce cell type-specific KOs (*Cre$^{+/-}$*, *Mgll$^{loxP/loxP}$*) and littermate controls (*Cre$^{-/-}$*, *Mgll$^{loxP/loxP}$*). Eno2-Cre, GFAP-Cre, and Lysm-Cre mice were also crossed to Rosa26-tdTomato reporter mice (Jax stock #007909) to validate Cre recombinase expression. PCR genotyping of genomic tail DNA was performed using 5'-ccagctaaacatgcttcatcgtcgg-3' and 5'- ccttctctacacctgcggtgctaac-3', which amplify a 356-bp product in cre-expressing mice, as well as 5'- cacctgtctttggagctc ccacc-3', 5'-cctttctttagggagagtccactgaatgtg-3', and 5'-ggcagcactgacaaatgtgtctgag-3', which amplify a 415-bp product in wild-type mice, a 533-bp product in mice with the MAGL floxed allele, and a 598-bp product in mice with the MAGL null allele.

Primary neuron, astrocyte, and microglia cultures. The primary cell culture protocols

used in this study were approved by the Scripps Research Institute Institutional Animal Care and Use Committee. Cortico-hippocampal neurons were prepared from embryonic day 18 mice from the different MAGL conditional lines as needed. Cortices/hippocampi were dissected, freed of meninges, and dissociated by incubation in Papain/DNase for 20 minutes at 37 °C followed by trituration. Dissociated cortico-hippocampal neurons were then washed with DMEM media supplemented with 10% FBS and 2 mM glutamine, prior to seeding them onto poly-D-lysine coated 10 cm culture dishes in neurobasal medium containing 2% B27 supplement, 2 mM glutamine, and 5 μM 5-fluoro-2′-deoxyuridine at a density of 8 x 10^6 cells/dish. A third of the media was exchanged twice per week. Neurons were harvested for proteome isolation after 16 days *in vitro*, at which point cultures contained <3% of non-neuronal cells.

Microglia were derived from mixed glial cultures prepared from postnatal day 2-3 mouse forebrains from the different MAGL conditional lines as needed. Briefly, forebrains were dissected, stripped of meninges, and digested in papain/DNAse (20 minutes at 37 °C) followed by 0.25% trypsin (15 min at 37 °C) and trituration. Dissociated cells were then cultured for 10 days in poly-D-lysine coated T75 tissue culture flasks in DMEM media supplemented with 10% FBS and 2 mM glutamine. After establishment of the astrocyte monolayer, the flasks were shaken for 2 h at 180 rpm to obtain the loosely attached microglia. Microglia were subsequently plated onto 10 cm dishes at a density of 3 x 10^6 cells/dish in Macrophage-SFM media (Gibco) supplemented with 1% FBS and 0.5 ng/ml of granulocyte macrophage-colony stimulating factor. The purity of these microglia cultures was >99% (**Figure S1F**), and cells were allowed to sit for at least 72 h prior to harvesting them for proteome isolation.

Following isolation of microglia, established mixed glial cultures were treated with 8 μM cytosine-arabinoside for 3-5 days to kill actively dividing cells (e.g. microglia, fibroblast), and generate an astrocyte monolayer with >85% purity (**Figure S1F**). These astrocytes were subsequently plated onto poly-D-lysine coated 10 cm dishes in DMEM media supplemented with 10% FBS and 2 mM glutamine, and allowed to become confluent. Upon reaching confluence, astrocytes were harvested for subsequent proteome isolation.

Preparation of mouse tissue and cell proteomes. 8-week old mice were anaesthetized with isoflurane, killed by cervical dislocation, and tissues harvested, immediately flash frozen in liquid nitrogen and kept frozen at −80 °C until use. For preparation of proteomes, tissues were homogenized in cold PBS using a bullet blender (Next Advance, Inc.) as per the manufacturer's instructions, followed by a low-speed spin (1,400 x *g*, 5 min) to remove debris, and ultracentrifugation (100,000 x *g*, 45 min) to separate membrane and cytosolic fractions. The supernatant was removed and saved as the soluble proteome, while the pellet was washed and resuspended in cold PBS by sonication and saved as the membrane proteome. Total protein concentration for each proteome was determined using a Bio-Rad Dc Protein Assay kit, and proteomes were kept at -80C until further use.

Activity-based protein profiling analysis. 50μL of 1mg/ml tissue membrane proteome were incubated with the broad-spectrum serine hydrolase probe FP-rhodamine (1 μM final concentration) for 30 min at room temperature. When necessary, proteomes were pre-treated with inhibitors for 1 hr at 37°C prior to addition of FP-rhodamine. Probe

labeling was terminated by quenching with 4x SDS/PAGE loading buffer, and labeled proteome samples were separated by SDS-PAGE [10% (wt/vol) acrylamide] and visualized by in-gel fluorescence scanning using a flatbed fluorescence scanner (Hitachi FMBio IIe). Rhodamine fluorescence is shown in grayscale, and optical density of the signals was determined using Image-J.

Western blotting. For western blotting, proteome samples were separated by SDS-PAGE [10% (wt/vol) acrylamide] and gels were transferred to a nitrocellulose membrane. The membrane was then blocked in 5% milk in 0.5% TBS-Tween and incubated overnight with MAGL (1:1000, rabbit, gift from Dr. Ken Mackie, Indiana University), Na^+/K^+ ATPase (1:1000, rabbit, Millipore), GluN1 glutamate receptor (1:1000, mouse, NeuroMab), α1 GABAA receptor (1:1000, mouse, NeuroMab), beta tubulin 3 (Tuj; 1:1000, chicken, Aves), GFAP (1:1000, rabbit, Abcam), and Iba1 (1:1000, rabbit, Wako) primary antibodies. Following incubation with IRdye680 secondary antibody (1:5,000, Licor Biosciences), membranes were visualized with a Licor Odyssey CLx near-infrared imager.

2-AG substrate hydrolysis assay. *In vitro* 2-AG hydrolysis was determined by liquid chromatography-mass spectrometry (LC-MS) monitoring of the generation of AA product. Briefly, 10 μg of brain membrane proteomes or primary cells from MAGL-T, -N, -A, and –MKO mice and wild-type littermates (2-month old, N=4/5 per genotype) were incubated with 100 μM 2-AG in PBS (100μl final volume) for 10 min. Reactions were quenched by addition of 300 μl of 2:1 (vol/vol) $CHCl_3$:MeOH doped with 0.5 nmoles of AA-d8 lipid standard, vortexed to mix, and spun at 2000 rpm x 5 min to separate

phases. The bottom organic phases was extracted and 20 μl were injected onto an Agilent 6460 triple quadrupole (QQQ) MS. Chromatography was performed on a 50 × 4.60 mm 5-μm Gemini C18 column (Phenomenex) coupled to a guard column (Gemini; C18; 4 × 3.0 mm; Phenomenex SecurityGuard cartridge). The LC method consisted of 0.5 mL/min of 100% buffer A [95:5 (vol/vol) H_2O:MeOH plus 0.1% (vol/vol) ammonium hydroxide] for 1.5 min, 0.5 mL/min linear gradient to 100% buffer B [65:35:5 (vol/vol) iPrOH:MeOH:H_2O plus 0.1% (vol/vol) ammonium hydroxide] over 5 min, 0.5 mL/min 100% buffer B for 3 min, and equilibration with 0.5 mL/min 100% buffer A for 1 min (10.5 min total run time). MS analysis was performed in negative scanning mode with an electrospray ionization (ESI) source using the precursor to product ion transition and collision energies for AA and AA-d_8 shown in **Table S1**. Dwell times for each lipid were set to 100 ms, and the following MS parameters were used: capillary voltage = 3.5 kV, drying gas temperature = 350 °C, drying gas flow rate = 9 L/min, and nebulizer pressure= 50 psi, sheath gas temperature = 375 °C, and sheath gas flow rate = 12 L/min. AA release was quantified by measuring the area under the peak in comparison with the AA-d_8 internal standard and correcting for non-enzymatically formed AA present in heat inactivated (10 min at 90 °C) control reactions, and relative 2-AG hydrolytic activity for conditional $MAGL^{-/-}$ proteomes was calculated by comparing to activity of wild-type proteomes.

Slice preparation and electrophysiology. Mice were anaesthetized by isoflurane inhalation and decapitated. Parasagittal cerebellar slices (250 μm thick) were prepared from 10- to 14-day-old mice, and transverse hippocampal slices were prepared from 20- to 30-day-old mice. Slices were prepared at 4-6°C in a sucrose-based solution

containing (in mM): 78 NaCl, 68 sucrose, 26 $NaHCO_3$, 2.5 KCl, 1.25 NaH_2PO_4, 2 $CaCl_2$, 2 $MgCl_2$ and 25 glucose. Slices were incubated for 30-40 min in sucrose solution and then transferred and stored in the artificial cerebrospinal fluid (ACSF) containing (in mM): 119 NaCl, 2.5 KCl, 2.5 $CaCl_2$, 1 $MgCl_2$, 1.25 NaH_2PO_4, 26 $NaHCO_3$, and 10 glucose. All solutions were saturated with 95% O_2 and 5% CO_2.

Whole-cell voltage-clamp recordings were made from cerebellar Purkinje cells (PCs) and hippocampal CA1 pyramidal neurons as described previously (Pan et al., 2009; Zhong et al., 2011). Excitatory postsynaptic currents (EPSCs) were recorded from cerebellar Purkinje cells while parallel fibers (PFs) were stimulated with a bipolar tungsten stimulation electrode (WPI) that was placed in the molecular layer. PF-EPSCs showed graded responses and exhibited paired-pulse facilitation (30-50 ms intervals) (Kreitzer and Regehr, 2001). $GABA_A$ receptor blocker picrotoxin (50 μM) was present in the ACSF. Glass pipettes (3-5 MΩ) were filled with an internal solution containing (in mM): 130 cesium methanesulfonate, 10 CsCl, 5 QX-314, 10 HEPES, 0.2 EGTA, 2 $MgCl_2$, 4 Mg-ATP, 0.3 Na_2GTP, and 10 Na_2-phosphocreatine (pH 7.2 with CsOH). EPSCs were evoked by electrical stimulation at 4 s intervals. DSE was induced by a brief depolarization (1 s from -70 mV to 0 mV). Inhibitory postsynaptic currents (IPSCs) were recorded from CA1 pyramidal neurons in hippocampal slices. AMPA receptor antagonist CNQX (20 μM) and NMDA receptor antagonist D-2-amino-5-phosphonovaleric acid (D-AP-5, 20 μM) were present in the ACSF. The pipettes were filled with an internal solution containing (in mM): 100 K-gluconate, 50 KCl, 0.1 $CaCl_2$, 1 EGTA-Na_4, 2 $MgCl_2$, 2 Mg-ATP, 0.3 Na_2GTP, and 10 HEPES at pH 7.2 (with KOH). To

induce DSI, the CA1 pyramidal neurons were depolarized from -70 mV to 0 mV for 5 s, and IPSCs were evoked at 4 s intervals.

CB_1R cross-tolerance *in vivo* behavioral assays. To examine CB_1R cross-tolerance in MAGL-TKO, -NKO and -AKOs and wild-type littermates, two month-old mice (N=7-8 per genotype, mixed sex) were evaluated for cannabimimetic responses following injection with WIN55,212-2. Specifically we assessed catalepsy in the bar test, antinociception in the tail immersion test at 56 °C, and hypothermia. Briefly, catalepsy was assessed on a bar 0.7 cm in diameter placed 4.5 cm off of the ground. The mouse was placed with its front paws on the bar and the amount of time it remained immobile (with the exception of respiratory movements) within a 60 s window was recorded. The assay was stopped after 60 s, or after the fourth time the mouse moved off the bar. Note that no differences in catalepsy were seen for any of our conditional $MAGL^{-/-}$ lines and these data are not shown. Nociception was assessed by holding each mouse and submerging 1 cm of its tail into a 56 °C water bath. The latency for the mouse to withdraw its tail was scored. Hypothermia was determined by measuring each mouse's rectal temperature with a rectal thermometer. Note that to reduce the number of mice required for these studies, we evaluated dose-response relationships using a cumulative dosing regimen in which baseline behavioral endpoints were assessed, injections were given every 40 min, and subjects were evaluated for each measure 30 min after each injection, with the entire dose-response assessment being completed in less than 4 h.

Agonist-Stimulated [^{35}S]GTPγS Binding. Tissue samples were thawed and homogenized in 20 ml ice-cold Buffer A (50 mM Tris-HCl, 3 mM $MgCl_2$, 1 mM EGTA, pH 7.4) on the day of assay. The sample was then centrifuged at 48,000 x *g* at 4°C for 10 min, resuspended in Buffer B (50 mM Tris-HCl, 3 mM $MgCl_2$, 0.2 mM EGTA, 100 mM NaCl, pH 7.4), and centrifuged at 48,000 x *g*. Membranes were resuspended in Buffer B, protein concentrations were determined, and membranes were pre-incubated for 10 min at 30 ˚C with adenosine deaminase (4 mU/ml) to remove endogenous adenosine. Membranes (5-10 μg) were then incubated at 30°C for 2 hr in Buffer A with 1 g/L bovine serum albumin (BSA), 0.8 mU/ml adenosine deaminase, 30 μM GDP, 0.1 nM [^{35}S]GTPγS and varying concentrations of CP55,940 in a 0.5 ml total volume. Basal binding was determined in the absence of agonist, and nonspecific binding was measured in the presence of 20 μM unlabeled GTPγS. All data reported are derived from specific binding. The reaction was terminated by rapid filtration under vacuum through GF/B glass fiber filters, followed by 3 washes with cold (4°C) Tris buffer (50 mM Tris-HCl, pH 7.4). Bound radioactivity was determined by liquid scintillation spectrophotometry at 95% efficiency for ^{35}S after extraction of the filters in scintillation fluid.

Lipid measurements. Metabolite levels were quantified by multiple reaction monitoring (MRM) of each lipid species using and Agilent 6460 QQQ instrument. 2 month-old MAGL-TKO, -NKO, -AKO, and -MKOs were injected intraperitoneally (ip) with LPS in PBS (20mg/kg) or with PBS vehicle alone. 6 hours post-injection, mice were sacrificed by cervical dislocation, and their brains rapidly removed and immediately flash frozen in liquid nitrogen. One brain hemisphere was then weighted and dounce homogenized in 8

ml of cold 2:1:1 (v/v/v) $CHCl_3$:MeOH:PBS doped with the following lipid standards: 1 nmol of 2-AG-d_5, 0.5 nmol of AEA-d_4, 1 nmol of AA-d_8 and 0.5 nmol of PGE2-d_9. Note that brains were not allowed to thaw prior to contact with organic solvents. Brain homogenates were vortexed and centrifuged at 2,000 rpm for 5 min. The organic bottom fraction was carefully collected, and the remaining solution was re-extracted by adding another 2 ml of $CHCl_3$ with 20μl of formic. The organic fractions from both extractions were combined, and dried under a nitrogen stream. Lipids were resolubilized in 200μl of 1:1 (v/v) $CHCl_3$:MeOH, 10 μl of which were injected for mass spectrometry analysis.

For cultured microglia LPS studies, 3 x 10^6 cells were treated with 100 ng/ml of LPS for 4 hrs. Lipids were then extracted from cells by scraping them from dish in 1.1 ml of cold PBS, of which 100 μl were saved to measure protein concentration for normalization, prior to re-scraping with 1 ml of cold MeOH. The 2 mL of cell lysate were then transferred to 2 mL of $CHCl_3$ with 20μl of formic acid and the following lipid standards: 0.5 nmol of 2-AG-d_5, 0.25 nmol of AEA-d_4, 0.5 nmol AA-d_8, and 0.5 nmol of PGE2-d_9. After centrifugation at 2,000 rpm for 5 min, the organic bottom fraction was carefully collected and dried under a nitrogen stream. Lipids were resolubilized in 140μl of 1:1 (v/v) $CHCl_3$:MeOH, 20 μl of which were injected for mass spectrometry analysis.

LC separation of lipid metabolites was performed on a 50 × 4.60 mm 5-μm Gemini C18 column (Phenomenex) coupled to a guard column (Gemini; C18; 4 × 3.0 mm; Phenomenex SecurityGuard cartridge). Mobile phase A consisted of 95:5 (vol/vol) H_2O:MeOH and mobile phase B consisted of 60:35:5 (vol/vol) iPrOH:MeOH:H_2O, with 0.1% formic acid or ammonium hydroxide added to both mobile phases to assist in ion

formation in positive and negative ionization modes, respectively. For the targeted detection of MAGs and NAEs in positive mode, each run started at 0.1 mL/min of 100% A. At 5 min, the solvent was immediately changed to 60% B with a flow rate of 0.4 mL/min and increased linearly to 100% B over 15 min. 100% B was allowed to flow at 0.5 mL/min for an additional 8 min prior to equilibrating for 3 min with 100% A at 0.5 mL/min. For targeted detection of eicosanoids and fatty acids in negative mode, each run started at 0.1 mL/min of 100% A. At 3 min, the flow rate was increased to 0.4 mL/min with a linear increase of solvent B to 100 % over 17 min. 100% B was allowed to flow at 0.5mL/min for 7 min prior to equilibrating for 3 min with 100% A at 0.5 mL/min. MS analysis was performed in either positive or negative scanning mode with an electrospray ionization (ESI) source, and the precursor to product ion transitions and collision energies for different metabolites shown in **Table S1** were used. Dwell times for each lipid were set to 100 ms, and the following MS parameters were used: capillary voltage = 3.5 kV, drying gas temperature = 350 °C, drying gas flow rate = 9 L/min, and nebulizer pressure= 50 psi, sheath gas temperature = 375 °C, and sheath gas flow rate = 12 L/min. Metabolite species were quantified by measuring the area under the peak in comparison with the appropriate unnatural internal standard and normalizing for wet tissue weight.

Cytokine analysis. Cytokines were measured using a DuoSet ELISA kit (R&D systems) as per the manufacturer's instructions. Brains were homogenized in cold PBS in the presence of 1 x protease inhibitor cocktail (Roche) using a bullet blender (Next Advance, Inc.), followed by a low-speed spin (1,400 x *g*, 5 min) to remove debris, and ultracentrifugation (100,000 x *g*, 45 min) to separate membrane and cytosolic fractions.

The supernatant from this ultracentrifugation (the mouse brain soluble proteome) was used in the assay. For cultured microglia, 100 μl of media were used in the assay.

Neuron-astrocyte transwell co-culture studies. Neurons and astrocytes were co-cultured in 10 cm transwell dishes with polycarbonate membrane permeable supports with a 0.4 mm pore size (Costar). Purified astrocytes (see above) were plated onto the membrane permeable supports following coating with poly-D-lysine, and maintained in DMEM media supplemented with 10% FBS and 2 mM glutamine until they reached confluency (5-7 days). At this point astrocytes on the membrane permeable supports were transferred to a separate 10 cm dish with neurobasal medium containing 2% B27 supplement, 2 mM glutamine, and 5 μM 5-fluoro-2′-deoxyuridine for 24 hours. During this time cortico-hippocampal neurons were prepared from embryonic day 18 $MAGL^{+/+}$ or $MAGL^{-/-}$ mice as described above and plated onto the transwell dishes at a density of 8 x 10^6 cells/dish. After allowing neurons to settle overnight, astrocytes on the membrane permeable supports were returned to the transwell dishes and co-cultures were maintained for 16 days *in vitro*. A third of the media was changed two times per week.

For AA-d_8 labeling experiments, co-cultures were allowed to mature for 12 days at which point astrocytes on the membrane permeable supports were transferred to a separate 10 cm dish for 48 hours. AA-d_8 conjugated to BSA prepared as described elsewhere (Rouzer et al., 2006) was then added to the media of neurons or astrocytes as needed at a final concentration of 2.5 mg/mL of BSA and 10 μg/ml of AA-d_8. After 48 hours of incubation, cells were thoroughly washed with warm media, the media fully replaced, and neurons and astrocytes co-cultured together for another 36 hours.

Lipids were extracted from each cell type separately by scraping cells from the transwell dish (for neurons) or from the permeable membrane support being held in a separate 10 cm dish (for astrocytes) in 1 ml of cold PBS and 1 ml of cold MeOH. The 2 mL of cell lysate were then transferred to 2 mL of $CHCl_3$ with 20μl of formic acid and the following lipid standards: 1 nmol of 2-AG-d_5, 0.5 nmol of AEA-d_4, AA-d_8 (replaced with 1nmol of PDA in AA-d8 labeling experiments) and 0.5 nmol of PGE2-d_9. After centrifugation at 2,000 rpm for 5 min, the organic bottom fraction was carefully collected and dried under a nitrogen stream. Lipids were resolubilized in 140μl of 1:1 (v/v) $CHCl_3$:MeOH, 20 μl of which were injected for mass spectrometry analysis. 5 ml of media from each transwell dish were also extracted in an analogous manner by combining with 5 ml of MeOH and 10 ml of $CHCl_3$.

Immunohistochemistry. Mice were deeply anesthetized using isoflurane and perfused with PBS followed by 4% (wt/vol) paraformaldehyde. Brains were then carefully dissected, postfixed in 4% paraformaldehyde overnight, cryoprotected in 30% (wt/vol) sucrose, and rapidly frozen on dry ice. Free floating coronal sections 40 μm in thickness were cut on a Leica CM1850 cryostat. For examination of microglial activation, frozen, free-floating sections were blocked with Bloxall (Vector labs, 10 min) and 0.2% Triton-X100 and 3% goat serum in PBS (blocking solution, 1 hr) prior to O/N incubation at 4 °C with a rabbit anti-ionized calcium-binding adaptor molecule (Iba)1 primary antibody (1:500 dilution in blocking solution; Wako). Sections were then incubated with secondary antibody (anti-rabbit biotin; Vector Laboratories; 1:300 dilution of 1.5 mg/mL stock) in 0.5% (wt/vol) BSA in 0.1 M PB for 1 h at room temperature and developed with ABC Elite Vectastain (Vector Laboratories). After staining, sections were mounted in

Permount and imaged using a Leica SCN400 whole slide scanner. Images were processed using ImageJ and Gimp using global adjustments in brightness and contrast. Iba1-positive microglia were quantified in matching sections from at least 5 mice per genotype using ImageJ particle analyzer. For examination of cre-induced expression of tdTomato, frozen, free-floating sections were blocked with 0.2% Triton-X100 and 3% goat serum in PBS (blocking solution, 1 hr) prior to O/N incubation at 4 °C with rabbit anti-NeuN (1:500; Abcam), rabbit anti-GFAP (1:500; Abcam) or a rabbit anti-Iba1 (1:500; Wako) primary antibodies. Sections were then incubated with secondary antibodies (anti-rabbit Alexa 488; Jackson Immunoresearch; 1:300 dilution) in blocking solution for 1 h at room temperature. After staining, sections were mounted in Vectashield hardset (Vector laboratories) and imaged using a Zeiss LSM 780 scanning confocal microscope. Images were processed in Zen, ImageJ, and Photoshop using global adjustments in brightness and contrast. TdTomato positive neurons, astrocytes, and microglia were quantified in matching sections from 2 mice per genotype using ImageJ.

Data Analysis and Statistics: Data are shown as the mean ± SEM. All statistical analyses were conducted using Excel or GraphPad Prism. A Student's t test (unpaired, two-tailed) was used to determine differences between two groups. A P value less than 0.05 was considered significant. For multi-group comparisons, 1-way ANOVA with post hoc Sidak's multiple comparison test was computed using a P-value threshold of 0.05.

For electrophysiology experiments, data are presented as the mean ± SEM. EPSC amplitudes were normalized to the baseline. The decay time constant (τ) of DSE was measured using a single exponential function of $y = y_0 + k \times \exp(-x/\tau)$. The

magnitude of DSE was calculated as follows: DSE(%) = 100 x [1- (mean of 3 EPSCs after depolarization/mean of 5 EPSCs before depolarization)]. Values of 2-3 DSE trials were averaged for each neuron. Data sets were compared with Student's *t*-test. Results were considered to be significant at $p < 0.05$.

For [^{35}S]GTPγS experiments, binding was assayed in triplicate and data are reported as mean ± SEM. % Stimulation = (agonist-stimulated – basal [^{35}S]GTPγS binding) / basal [^{35}S]GTPγS binding x 100%. Concentration-effect curves were analyzed by nonlinear regression to yield E_{max} and EC_{50} values using GraphPad/Prism 5.0 software. All data were subjected to ANOVA with post-hoc Dunnett's test to determine significant differences between conditional knockout and control mice using GraphPad/Prism 5.0 software.

Table S1, related to Figures 1, 4, and 5. Precursor to product ion transition and collision energies for all lipids measured by MRM-MS.

Species	Precursor	Product	Collision Energy	Polarity
2-AG	379	287	8	Positive
2AG-d_5	384	287	8	Positive
2AG-d_8	387	295	8	Positive
AEA	348	62	11	Positive
AEA-d_4	352	66	11	Positive
AA	303	303	0	Negative
AA-d_8	311.2	311.2	0	Negative
PGE_2/D_2	351	271	4	Negative
PGE_2-d_9	360.5	280	4	Negative
SAG	662.5	341	40	Positive
SAG-d_8	670.5	341	40	Positive
PC C18:0/C20:4	810.6	184.1	15	Positive
PC C18:0/C20:4-d_8	818.6	184.1	15	Positive
PI C18:0/C20:4	885	241.3	40	Negative
PI C18:0/C20:4-d_8	893	241.3	40	Negative
PS C18:0/C20:4	810.5	283.3	35	Negative
PS C18:0/C20:4-d_8	818.5	283.3	35	Negative

Supplemental References

Clausen, B.E., Burkhardt, C., Reith, W., Renkawitz, R., and Forster, I. (1999). Conditional gene targeting in macrophages and granulocytes using LysMcre mice. Transgenic Res *8*, 265-277.

Frugier, T., Tiziano, F.D., Cifuentes-Diaz, C., Miniou, P., Roblot, N., Dierich, A., Le Meur, M., and Melki, J. (2000). Nuclear targeting defect of SMN lacking the C-terminus in a mouse model of spinal muscular atrophy. Hum Mol Genet *9*, 849-858.

Kreitzer, A.C., and Regehr, W.G. (2001). Retrograde inhibition of presynaptic calcium influx by endogenous cannabinoids at excitatory synapses onto Purkinje cells. Neuron *29*, 717-727.

Otto, C., Fuchs, I., Kauselmann, G., Kern, H., Zevnik, B., Andreasen, P., Schwarz, G., Altmann, H., Klewer, M., Schoor, M.*, et al.* (2009). GPR30 does not mediate estrogenic responses in reproductive organs in mice. Biol Reprod *80*, 34-41.

Pan, B., Wang, W., Long, J.Z., Sun, D., Hillard, C.J., Cravatt, B.F., and Liu, Q.S. (2009). Blockade of 2-arachidonoylglycerol hydrolysis by selective monoacylglycerol lipase inhibitor 4-nitrophenyl 4-(dibenzo[d][1,3]dioxol-5-yl(hydroxy)methyl)piperidine-1-carboxylate (JZL184) Enhances retrograde endocannabinoid signaling. J Pharmacol Exp Ther *331*, 591-597.

Patricelli, M.P., Giang, D.K., Stamp, L.M., and Burbaum, J.J. (2001). Direct visualization of serine hydrolase activities in complex proteomes using fluorescent active site-directed probes. Proteomics *1*, 1067-1071.

Rouzer, C.A., Ivanova, P.T., Byrne, M.O., Milne, S.B., Marnett, L.J., and Brown, H.A. (2006). Lipid profiling reveals arachidonate deficiency in RAW264.7 cells: Structural and functional implications. Biochemistry *45*, 14795-14808.

Tao, J., Wu, H., Lin, Q., Wei, W., Lu, X.H., Cantle, J.P., Ao, Y., Olsen, R.W., Yang, X.W., Mody, I.*, et al.* (2011). Deletion of astroglial Dicer causes non-cell-autonomous neuronal dysfunction and degeneration. J Neurosci *31*, 8306-8319.

Zhong, P., Pan, B., Gao, X.P., Blankman, J.L., Cravatt, B.F., and Liu, Q.S. (2011). Genetic deletion of monoacylglycerol lipase alters endocannabinoid-mediated retrograde synaptic depression in the cerebellum. J Physiol *589*, 4847-4855.